Characterizing and Mitigating Small-Diameter Tool Wear in Nickel-Based Superalloy Machining

by

Alexander Sparry Brush

Submitted to the Department of Mechanical Engineering
in partial fulfillment of the requirements for the degree of

MASTER OF ENGINEERING IN ADVANCED MANUFACTURING AND DESIGN

at the

MASSACHUSETTS INSTITUTE OF TECHNOLOGY

August 2025

Authored by: Alexander Sparry Brush
Department of Mechanical Engineering
August 8th, 2025

Certified by: David E. Hardt
Ralph E. and Eloise F. Cross Professor of Mechanical Engineering
Thesis Supervisor

Accepted by: Nicholas Hadjiconstantinou
Professor of Mechanical Engineering
Chairman, Department Committee on Graduate Thesis

This page was intentionally left blank

Characterizing and Mitigating Small-Diameter Tool Wear in Nickel-Based Superalloy Machining

by

Alexander Sparry Brush

Submitted to the Department of Mechanical Engineering
on August 8th, 2025 in partial fulfillment of the requirements for the degree of

MASTER OF ENGINEERING IN ADVANCED MANUFACTURING AND DESIGN

Abstract

This thesis investigates tool failure in the micromachining of single-crystalline René N4 turbine blades coated with ceramic thermal barrier layers. The work done in this thesis was promoted through a partnership between Massachusetts Institute of Technology (MIT) and GE Vernova. This thesis is complemented by the thesis written by Luke Placzek. Together these works offer a comprehensive case study in process analysis and manufacturing optimization.

This thesis begins with groundwork to document tool failure mechanisms and frequencies through photographic analysis. This was done alongside a study of historical data to analyze tool breakage frequency in the context of the turbine blade. Based on these insights, an Analysis of Variance (ANOVA) test followed by a Tukey's Honestly Significant Difference (HSD) test identified statistically significant differences in tool breakage rates across machines and rows. A detailed study of tool wear progression was conducted to better understand how small-diameter endmills wear when machining the nickel-based superalloy René N4. Utilizing all these findings, an updated tool path was created to optimize tool life

This work lays the foundation for an improved machining strategy to reduce tool breakage in manufacturing turbine blades. Estimations show that the refined CAM strategies may reduce tool breakage by roughly 33 percent. Preliminary models estimate the implementation of the suggested improvements will save GE Vernova 2.5 million dollars per year.

Thesis supervisor: Dave E. Hardt
Title: Ralph E. and Eloise F. Cross Professor of Mechanical Engineering

This page was intentionally left blank

Acknowledgements

I would like to thank my parents, Diane Brush and Charles Brush, for their constant support not only throughout my graduate studies, but throughout my entire life. Regardless of what you are doing or where you are you have always had my back. You always answer my FaceTime calls no matter what you are in the middle of doing, and we end up having a long talk that often drifts into technical issues I am facing. I know that the majority of the time these topics are less than thrilling, but you always patiently listened and discussed it with me and that means the world to me.

I would also like to express gratitude to Prof. Dave Hardt for his guidance and mentorship throughout this project. Our frequent meetings helped me stay on track and allowed me to tap into your wide range of manufacturing experience and knowledge. Your perceptive questioning and feedback challenged me to think through problems more critically and view them from new perspectives. I am very incredibly grateful for your patience and encouragement, and I am positive that the skills I have gained through your support will continuously influence my work throughout my career.

A huge thank you also goes to everyone at GE Vernova who helped with this project. There are so many people that greatly contributed by answering repeated follow-up questions about the work. Special thanks to the workers on the factory floor who were so welcoming and helped point towards real issues faster than any data analysis could.

This page was intentionally left blank

Table of Contents

List of Figures

This page was intentionally left blank

List of Tables

This page was intentionally left blank

Chapter 1 Introduction

1.1 Motivation and Problem Statement

Turbine blades used in power generation represent one of the most challenging applications in precision manufacturing. These blades are used in the 7HA.03 gas turbine, the most efficient gas turbine in the world, designed for cutting edge combined-cycle power generation [1]. The blades in these turbines operate under extreme temperatures and mechanical loads, and they require a variety of precisely machined features. Among the most critical of these features are rows of small-diameter diffuser holes. These holes, often with complex geometries and small diameters, are essential for internal cooling and thermal protection of the blade surface during operation. As the turbine is operating, air is pumped through the diffuser holes, creating a boundary layer between the ambient air in the turbine and the blade. This boundary layer is important because while the high internal temperatures are important for turbine efficiency, they exceed the melting temperature of the blades [2]. Due to their critical function, the diffuser holes must be produced to extremely tight positional and angular tolerances to ensure proper flow behavior. However, each blade has slightly different geometries due to casting and coating variation, and each row of holes has a different number of holes, each with custom geometries to conform to the complex shape of the blade. This results in a complex, time-consuming manufacturing process faced by GE Vernova.

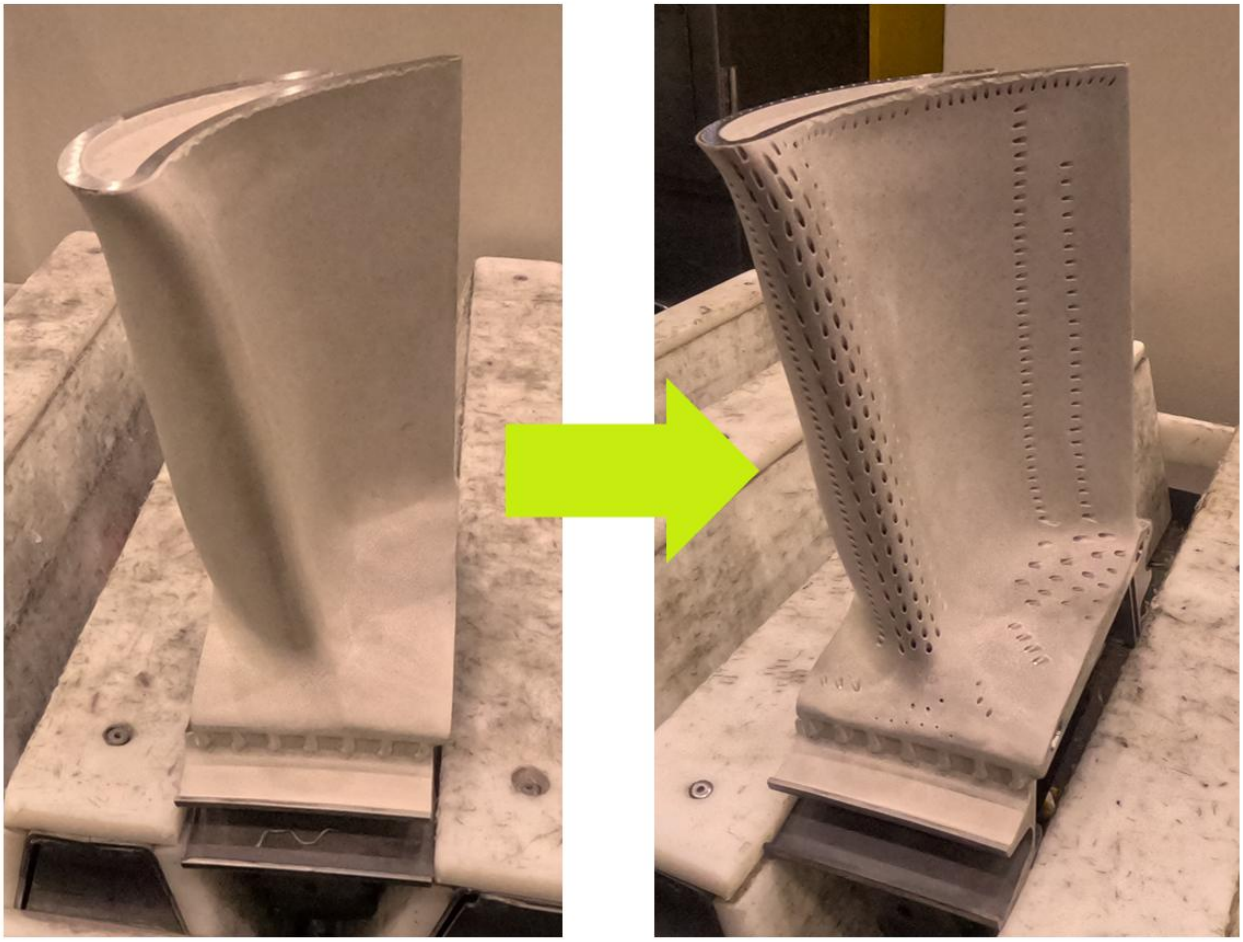

Figure 1.1: Turbine blade before (left) and after (right) the hole milling process.

Manufacturing diffuser holes in turbine blades involves micromachining with small-diameter end mills, often tapered to reach into angled geometries. The current process involves an initial hole cut using a roughing tapered end mill, followed by a second operation with a smaller diameter tool to refine the hole and to reach into the smaller geometry. These tools are made of tungsten carbide with a protective coating, but their small geometry makes them highly susceptible to wear, chipping, and catastrophic breakage. This is further complicated by the materials involved: the blades are made out of a René N4, a proprietary single-crystalline nickel-based superalloy [3]. Due to the strength and wear resistance of superalloys, they are known for their poor machinability, low thermal conductivity, and strong work hardening behavior [4], [5]. In addition, the blades are coated in a ceramic thermal barrier layer, which presents an abrasive, brittle surface that traps heat during machining and further increases the likelihood of tool wear and damage during operation [6].

Tool breakage is a frequent occurrence in the process of machining diffuser holes. In a best-case scenario, a broken tool requires a rework of the diffuser hole it was operating on, and in a worst-case scenario it can lead to a scrapped part, each of which is valued at roughly five

times the cost of legacy blades. While the individual cost of a tool is relatively low, the total costs of increased cycle time and all the broken tools are substantial. On average, the current machining process used by GE Vernova results in approximately 60 tools broken per part, requiring roughly five extra hours of machining on a 24-hour process. With eight machines currently operating daily, this step in the manufacturing process is one of the biggest bottlenecks for GE Vernova.

Micromachining at this scale introduces unique challenges not seen in conventional machining. At very small diameters the tool is much more susceptible to minor spindle runout or fixturing variation, both of which can lead to tool fatigue [7]. As a result, even with careful process planning and optimized cutting parameters, microtool breakage can remain as a persistent failure. Much existing research focuses on tool life in controlled laboratory settings, where part geometries and toolpaths are highly repeatable. However, in real-world manufacturing settings involving complex parts, such as turbine blades, there are numerous uncontrolled sources of variation.

This thesis is motivated by the need to better understand microtool breakage from a statistical production-level perspective. Specifically, utilizing GE Vernova as a case study presents an opportunity to apply a standardized approach to categorizing tool breakage patterns and propose a solution tailored to a specific step in the manufacturing process of gas turbine blades. This thesis aims to apply a variety of statistical tools to compare breakage frequency and patterns across different machines, setups, and hole types. These methods offer a rigorous, data-driven approach to uncovering root causes of tool failure. This work is conducted in parallel with a collaborative thesis by Placzek [8], focusing on sensor-based detection of tool failure using microphones and vibration sensors along with a plan for identifying and quantifying trends in tool breakage. Both theses share a common methodology for categorizing and visualizing tool breakage events, and the combined effort aims to offer both reactive and proactive improvements to micromachining robustness.

1.2 Overview of Hole Machining Process

The hole machining process for turbine blades in this study was performed using a FANUC RoboDrill α-D21L*i*B5 Adv vertical machining center, paired with a Koma Precision TWA-130 rotary table. This configuration enables 5-axis positional control, allowing the tool to create complex features on the blade surface. Figure 1.2 shows a RoboDrill on the factory floor, with Figure 1.3 showing the rotary table mounted inside. The manufacturing cell currently includes eight RoboDrill machines, with plans to expand to 20 active units by the end of 2025. This growth in capacity emphasizes the importance of improving tool reliability and process robustness.

Figure 1.2: Drill through coating (DTC) RoboDrill machine line.

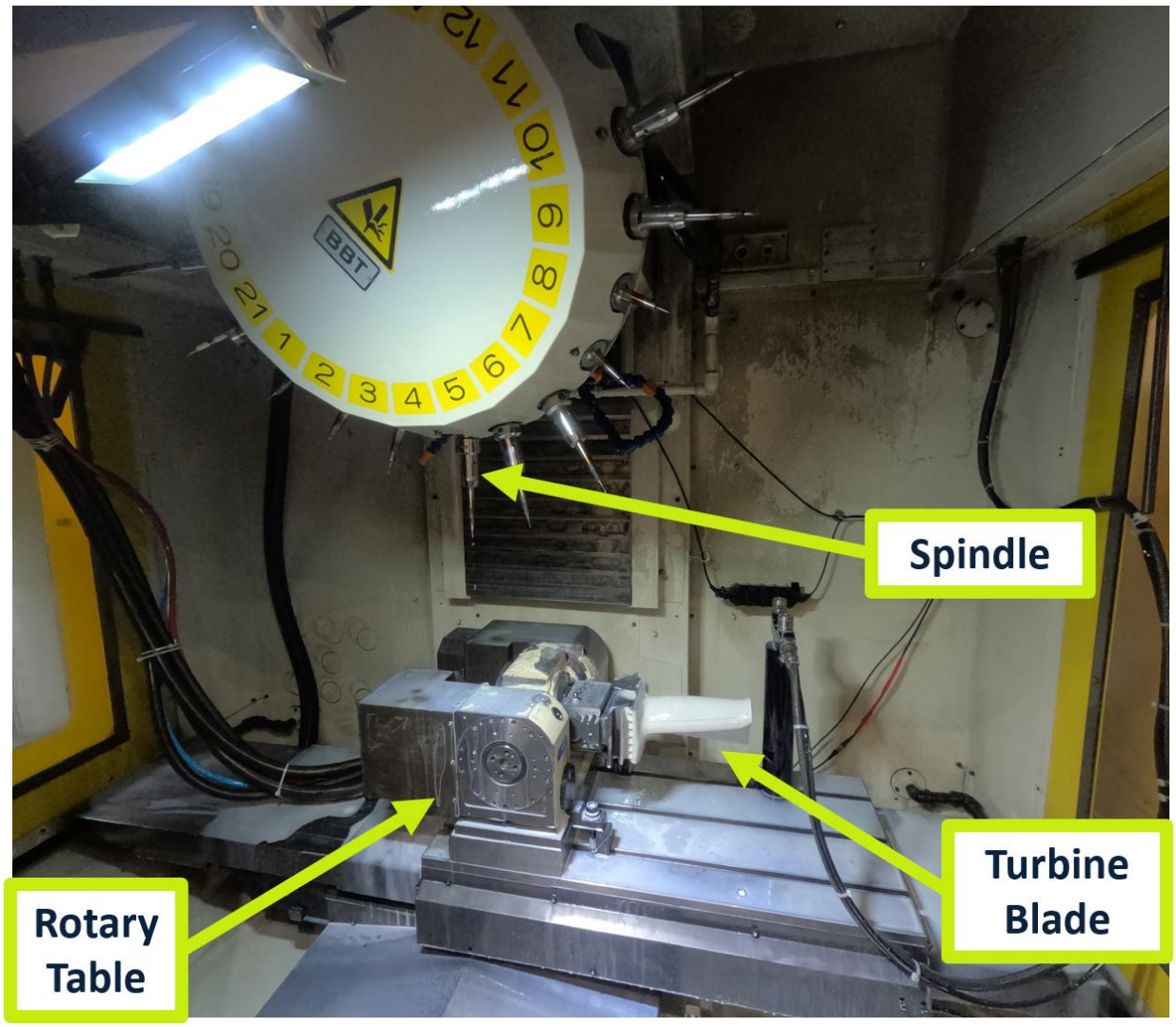

Figure 1.3: Rotary table holding turbine blade inside RoboDrill.

The process examined in this study involves machining small-diameter tapered holes into ceramic-coated superalloy turbine blades using tapered end mills in two sizes. The larger tool is referred to as the roughing tool and the smaller tool is identified as the finishing tool. Each tool is available in lengths of small, medium, and large, allowing for flexible reach depending on the blade orientation. This is necessary because the tool must approach the blade surface from varying angles depending on the holes geometry. To accommodate the extended reach requirements, a nested tool holding system is used. Each end mill is held within a heat-shrink tool holder, which is itself mounted inside a hydraulic tool holder. The length of the heat-shrink holder is varied to achieve the three lengths. The heat-shrink holder also features through-spindle coolant delivery, which ejects coolant through the contact face between the tool and the tool holder by means of thin channels.

To locate the blade accurately within the machine coordinate system, the RoboDrill uses a probing system. The machine then compares the probed part geometry against the nominal CAD model, imported from Siemens NX, and iteratively adjusts the part's orientation to achieve alignment within a set tolerance. This ensures that each hole is machined with respect to its intended surface normal, even in the presence of casting or coating variation.

Tool length is monitored using an integrated laser measurement system located within the RoboDrill enclosure. At the start of a tool's life, its length is measured. After each hole is machined, the tool is not fully remeasured; instead, time is saved by checking the tool at a length of 0.008 inches shorter than the original measurement. If the tool is found to be shorter than this threshold, it is automatically flagged as broken. If not, the machine continues to use the tool. In each machine, two to three of each tool type and length are loaded so the machine can continue operation after a tool breaks. After all copies of the same tool are broken, the machine waits for an operator to replace the tools. The operators keep a buffer of replacement tools by the machines to minimize downtime.

1.3 Small-Diameter Machining

1.3.1 Micromachining Fundamentals

Although the hole drilling process used in the application of turbine manufacturing does not strictly fall under the conventional definition of micromachining, it is close enough in scale that the principles of micromachining are directly relevant. While the exact bounds of micromachining in literature are unclear, many sources agree that micromachining can be defined as machining operations performed with tools smaller than half a millimeter, roughly 19.7 thousandths of an inch [9], [10], [11]. In this project, the tapered end mills are sized near the traditional definition of micromachining, and they exhibit failure modes, process sensitivities, and design constraints that are characteristic of micromachining.

Micromachining introduces additional complexities not typically encountered in conventional-scale machining. First and foremost, the small cross-sectional areas combined with high length-to-diameter (L:D) ratios make the tools much more prone to bending, deflection, and vibration, which can significantly affect cutting accuracy and cause tool breakage [9], [12]. Due to these constraints, micro tooling is often made of coated tungsten carbide because of its high strength and toughness [9], [13], [14]. In the current application, extended tool lengths are used to reach holes from various rotary orientations, amplifying misalignment and vibrations; this can cause brittle failure and therefore reduce the window of working process parameters.

A major distinction between micromachining and conventional machining lies in chip formation mechanisms. While chip formation at conventional scales is dominated by plastic deformation and well-understood shear mechanics, micromachining often exhibits ploughing or rubbing behavior when the uncut chip thickness is less than the minimum chip thickness [15]. This phenomenon reduces cutting efficiency and increases heat generation, therefore leading to premature tool wear.

Another critical issue in small-diameter machining is spindle runout. Small differences, such as a few thousandths of an inch of runout, can lead to unequal loading on the cutting edges, resulting in uneven wear and chatter [15]. Since the current process relies on a nested tool holder system for long reach tooling, minimizing runout and maintaining concentricity are essential for tool longevity and part quality. Runout-induced tool wear is a common cause of early tool failure in micromachining applications [16].

Thermal effects become increasingly significant in micromachining, with end mills experiencing high localized temperatures due to low mass, poor heat dissipation, and limited coolant penetration. In coated superalloy substrates, this is especially problematic because of the low thermal conductivity of the material and the thermal insulation provided by the ceramic coating. Sections 1.3.2 Machining in Superalloys and 1.3.3 Effects of Ceramic Coatings on Tool Performance will further describe the challenges of machining coated superalloys.

Micromachining requires higher machine accuracy than conventional machining. Using RoboDrills to machine turbine blades requires laser measurements and high-resolution nesting techniques to localize features on the part with sufficient precision. In the present application, the RoboDrill system is programmed with a custom nesting approach along with laser-based tool length measurements. These practices are drawn directly from the field of micromachining.

While the turbine blade hole machining process in this study exists near the boundary of micromachining and conventional machining, it clearly inherits the constraints of micromachining. Tool deflection, breakage, wear sensitivity, thermal stress, and high sensitivity to machine variation all apply. As such, understanding the principles of micromachining is essential for analyzing and improving this process. These fundamentals will serve as a foundation for later discussions of breakage behavior and statistical process analysis.

1.3.2 Machining in Superalloys

Superalloys, particularly those that are nickel-based, are engineered for use in extreme environments that demand high mechanical strength and thermal resistance. These materials are commonly used in turbine components due to their ability to maintain structural integrity at high temperatures, especially under cyclic loading. One such material is René N4, a nickel-based superalloy developed by the General Electric Company for turbine blade applications. In the turbine blade manufacturing process, René N4 is cast as a single crystal, meaning it has one consistent crystal structure throughout the component with no grain boundaries. The high strength and low thermal conductivity, while advantageous for performance, pose significant challenges for machining, especially with small diameter tooling [3], [5].

Research into both single-crystalline and polycrystalline nickel-based super alloys has identified several strategies for improving cutting performance. Although the focus in many of these studies is often on conventional-scale tools, the underlying methodologies remain relevant to small-diameter machining. Gonzalezet al. [17] analyzed ploughing in a single-crystal superalloy, concluding that lowering the feed rate was the main factor in reducing wear in small-diameter tools. However, feed rate needs to be experimentally optimized to not promote

ploughing. Gat et al. [18] confirms these findings, concluding from their study that the main factors, of those tested, that affect surface roughness are feed rate, spindle speed, and milling depth, in that order. In this instance, surface roughness is used as a measured output, but it can be assumed that these results will carry meaningful implications for tool life as well, since surface roughness is often indicative of underlying wear mechanisms and machining stability. Qiu et al. [19] documented the anisotropic properties of single-crystalline nickel-based superalloys, highlighting that the machinability changes as the material is cut along various crystal directions. This anisotropy causes variability in cutting forces, chip formation, and surface finish when machining the same material along different directions.

1.3.3 Effects of Ceramic Coatings on Tool Performance

Ceramic coatings on turbine blades serve as an insulator, protecting the blades from the extreme temperatures generated during turbine operation. These coatings are applied over a metallic bond coat and form a hard, brittle layer on the surface of the blade. However, in manufacturing, the thermal insulation, when combined with the low thermal conductivity of René N4, results in significant heat retention during cutting. This means that during machining most of the heat generated by shear and friction remains trapped within the cutting area, leading to tool wear. This is especially prevalent in small-diameter end mills that already struggle with limited heat dissipation and low thermal mass.

The brittle nature of ceramics introduces additional challenges to this machining process. Unlike ductile materials, ceramics exhibit low fracture toughness and poor resistance to shock, making them susceptible to edge chipping or crack propagation under intermittent cutting loads or small mechanical disturbances. Arif et al. [20] proposed an analytical method to determine cutting parameters in brittle materials such that material removal is defined by chip formation and not cracking, concluding that no one parameter affects ceramic milling quality, rather an experimentally determined ratio of feed rate and radial cutting depth optimizes surface finish. It is highlighted by Móricz et al. [21] that tool wear is one of the main issues when machining ceramics, especially because in a large-scale manufacturing operation it is not economical to stop a process to measure a tool and record the wear.

The presence of a ceramic thermal barrier coating atop a difficult-to-machine superalloy significantly increases the complexity of the diffuser hole manufacturing process. It elevates thermal loads and causes brittle interactions at the tool edge, both of which contribute to tool premature tool failure. These challenges motivate the need for both careful process parameter selection and advanced methods of monitoring and optimizing tool performance, as explored in this thesis.

1.4 Tool Failure and Breakage Mechanisms

1.4.1 Failure Modes in Small End Mills

Small-diameter carbide end mills, such as the roughing and finishing tools used in this study, are particularly susceptible to catastrophic tool failure due to their slender geometry and material limitations. A study by Ren et al. [11] on micro-milling investigated modeling the bending stress from a cutting operation to predict premature tool breakage. This study aimed to produce a breakage curve for small-diameter end mills, plotting feed per tooth against axial depth of cut. Supporting this, Lu et al. [22] proposes a method of estimating tool breakage through a stress analysis utilizing radial, tangential, and axial cutting forces. These studies illustrate how excessive feed per tooth or depth of cut can quickly drive the tool into catastrophic failure.

As discussed in Sections 1.3.2 Machining in Superalloys and 1.3.3 Effects of Ceramic Coatings on Tool Performance, thermal degradation is a common failure mode for this specialized machining. At high temperatures, metals soften, reducing the tools' toughness. Research by Acchar et al. [23] analyzed the mechanical properties of tungsten-carbide, highlighting that at operating temperatures above 600°C, the material develops microstructural defects which contribute to premature failure. Micro-scale cracks that develop in tools often quickly propagate, especially in five axis machining, due to dynamic loading of the tool [24]. Failure mechanisms such as axial loading and thermal degradation do not operate alone, but rather in sequence, collectively contributing to tool failure. Understanding the different mechanisms and interactions between them is essential for addressing tool reliability.

1.4.2 Breakage Progression

Tool failure in small-diameter milling can be difficult to analyze, however there are often stages of wear that progressively lead to failure. When using a new tool, there is often rapid initial wear which dulls the fine tip of the tool [25]. Saha et al. [26] concluded that the first 15 millimeters of cutting often dulls the tool due to friction. After this initial wear, it is noted that the tool follows a more gradual wear trend. Following the initial wear, the end mill length approximately follows a linear wear trend as the tool dulls [25]. This stage of tool wear is the longest stage and is where preventative countermeasures can most effectively be implemented to reduce tool breakage. Finally, accelerated wear leads to the end of the tool’s life. At this stage, catastrophic tool failure is often abrupt as increased loading shatters the carbide [27].

In the context of this thesis, understanding the progression of tool wear is critical because it is this fundamental behavior that will be tracked and analyzed when working towards a solution. Chapter 4 will track tool life and visualize the stages of wear found in literature.

1.5 Scope of Collaboration and Division of Work

This thesis represents a collaborative effort between Alexander Brush and Luke Placzek. The initial stages of the project, specifically the documentation of tool failure modes and the exploratory analysis of breakage trends, were investigated jointly. Both contributors were actively involved in the foundational analysis to understand the scope and nature of the problem at hand.

Following this joint effort, the focus of the work diverged into two complementary directions. Placzek [8] concentrated on the development of proactive monitoring systems, focusing on the groundwork for a machine learning model capable of in-situ monitoring. Both collaborators developed a live statistical process control (SPC) dashboard for tracking and identifying trends in tool breakage. These initiatives are designed to support long term process improvement. This thesis focuses on immediate interventions to address the identified tool reliability issues. The work done in each thesis together provide GE Vernova with a proposed immediate solution as well as tools to further solve the problem of tool breakage.

Chapter 2 Tool Failure Documentation

2.1 Introduction and Process Context

This chapter provides an analysis of tool failures encountered during the machining of cooling holes in single-crystal René N4 turbine blades coated with a ceramic thermal barrier. It begins with a description of the tooling setup and machine configuration, followed by a photographic analysis of both failed and intact end mills to categorize failure modes and frequencies. The goal is to establish a baseline understanding of the failures that are resulting from the current manufacturing process. This foundation is critical for guiding further investigation into the problem and proposing solutions.

This study was prioritized early in the project timeline to initially diagnose the tool failure problem. Upon the start of this project, there was limited quantitative knowledge about the distribution and characteristics of failures. By examining a representative sample of used and broken tools, it became possible to identify dominant failure mechanisms such as dulling, melting, and brittle fracture. This early insight shaped subsequent analysis, including the statistical analysis and the tool life wear test.

In this analysis, tools were not tracked back to specific machines, parts, or hole locations. The machining process is long and complex, involving hundreds of holes, and tool replacement is continuously performed by operators throughout the production process. Tracking each tool throughout its entire life cycle and mapping it to specific process variables would require a large time investment and planning, which was not feasible for this test. Instead, a random sample of broken tools was collected from a recycling container where all broken tools from this process. While this method limits the ability to draw direct correlations to process parameters, it provides an overview of tool failures to inform future investigations.

The results from this chapter serve as a baseline for the rest of the thesis. By identifying the most prevalent failure types and their relative frequencies, the study informs later chapters which further explore correlations between breakages and process variables.

2.2 Tooling Setup and Configuration

The tool holding system for this process is a multi-stage assembly designed to provide the reach required to machine holes at the required angles into the turbine blade. Each tool assembly begins with a hydraulic tool holder, which in turn secures a heat-shrink extension holder which holds the end mill. This modular approach enables a short, medium, and long length configuration for both the roughing and finishing tools. The varying lengths are necessary to reach holes positioned at different angles and depths as the part moves and rotates within the five-axis setup. As seen in Figure 2.1, 13 tools are loaded into the RoboDrill such that there are multiple of each tool configuration in the machine. Although 13 tools are loaded, far more are

broken per part, and therefore operators need to replace tools once all of one tool type have broken.

Figure 2.1: 13 tools held in RoboDrill turret for use during operation. The turret holds multiple of each type of tool to use when a tool breaks.

In this nested tool holder setup seen in Figure 2.2, the hydraulic holder is what directly mounts to the RoboDrill, and it securely mounts to the heat-shrink extension. Aligning the heat-shrink extension in the hydraulic holder is a precise process, but it only needs to be done once during the life of the heat-shrink extension. When tools break, the hydraulic and heat shrink holders stay connected and the end mill is replaced by an operator. The inner diameter of the heat-shrink extension is slightly smaller than the diameter of the carbide end mill, but when heated the extension expands, allowing the tool to be set, holding it firmly when cooled. Figure

2.3 shows each piece of the tool holder setup separated, and Figure 2.4 shows the three lengths of heat-shrink extension that are used in operation.

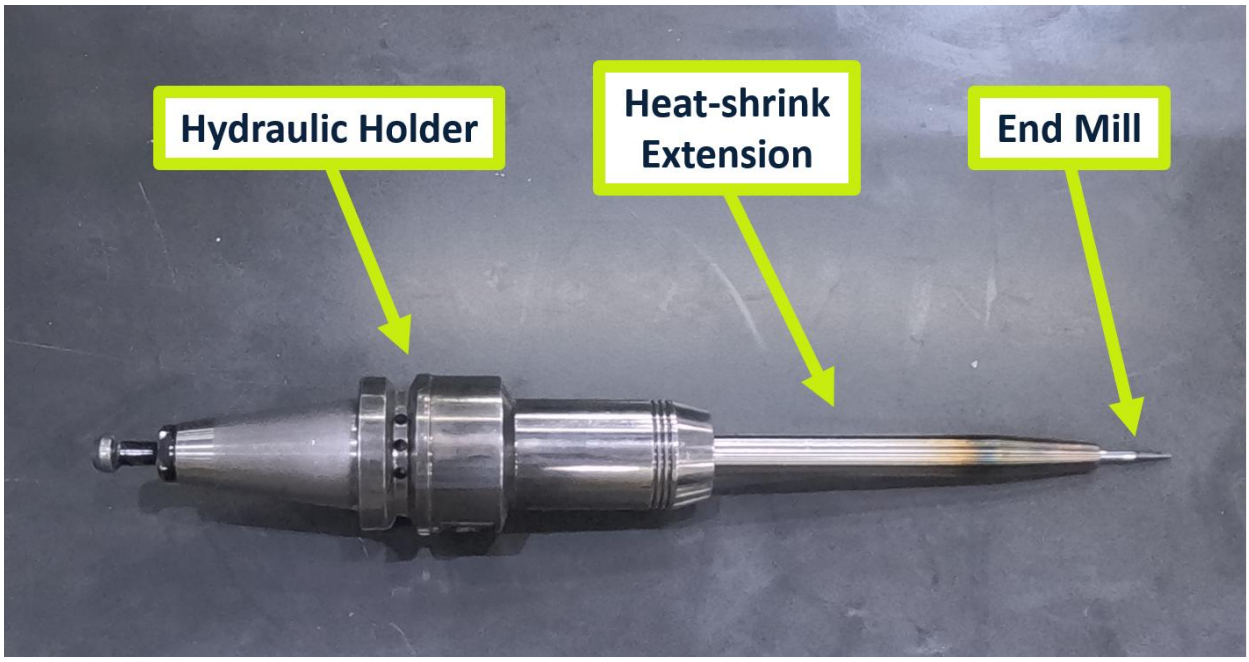

Figure 2.2: Long length tool holder setup.

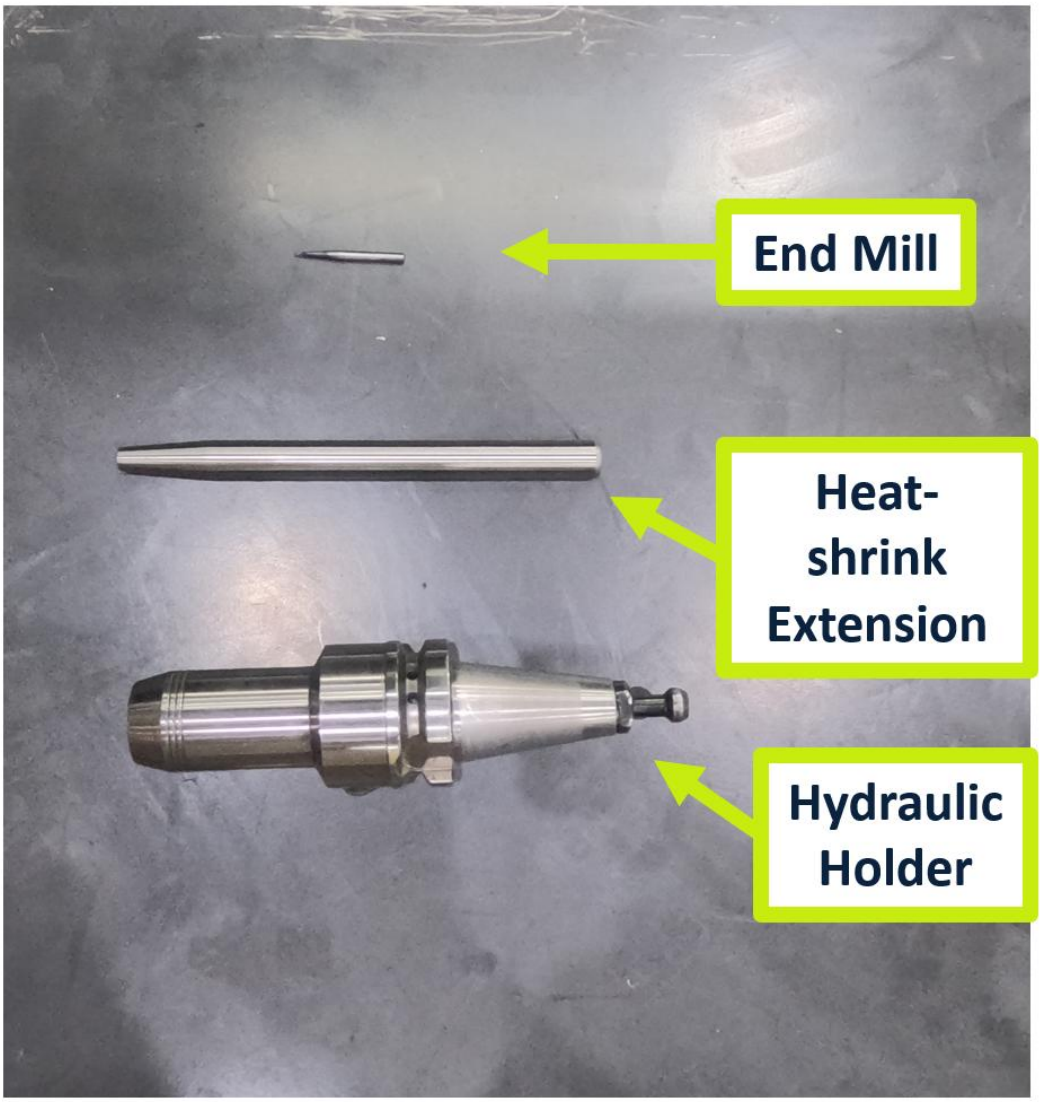

Figure 2.3: Long length tool holder separated into components.

Figure 2.4: Three lengths of heat shrink holders (large, medium, and small).

Coolant delivery is integrated throughout this assembly. Pressurized coolant enters the hydraulic holder through internal channels, flows through the heat-shrink holder, and exits at the boundary between the carbide end mill and the end of the heat shrink extension. This setup is necessary because the holes being milled are so small that applying coolant off-axis from the spindle will make it difficult for it to get to the cutting area.

2.3 Tool Failure Observations

2.3.1 Photographic Analysis of Broken and Intact Tools

To understand the variety and progression of tool failure modes encountered during the process of machining single-crystalline René N4 turbine blades, a photographic study was conducted using a representative selection of used and unused roughing and finishing carbide end mills. All failed tools were collected from a recycling bin where operators place tools identified by the RoboDrill as broken. Additionally, new tools were photographed immediately after being removed from the packaging, serving as a reference to compare varying levels of dull tools.

The first set of images focuses on roughing end mills, which perform the initial stage of hole creation in the blade, deeming them roughing tools. 30 roughing tools were photographed in this study, and a selection of three are displayed below, showcasing the three failure modes most common to this process. All images of broken tools used in this study can be seen in Appendix A. Of the three failure modes, one tool exhibits melted material near the tip, one shows significant dulling with rounded edges, and one has undergone catastrophic shattering.

To provide a reference, a new roughing end mill was photographed from orthogonal perspectives. Figure 2.5 shows that two flutes do not converge at the tip of the tool. Figure 2.6 shows the same tool as Figure 2.5, with the tool rotated 90° along the center axis to highlight the two flutes that do converge at the tip. The well-defined cutting edges in these images serve as a strong comparison point for assessing broken tools.

Figure 2.5: New roughing end mill showing the tips of each flute.

Figure 2.6: New roughing end mill rotated 90° to display a clean center point.

In the melted tool image, Figure 2.7, a gloss, darkened appearance can be seen near the cutting end, likely indicating thermal overload. This may have resulted from ineffective chip evacuation or localized heat accumulation due to poor coolant flow or excessive engagement time. Localized high temperatures are expected due to the thermal conductivity of both the superalloy and the ceramic coating. While this tool appears melted, it is possible that it shattered before melting, due to how much of the tool is missing. This is apparent when comparing with Figure 2.5 and Figure 2.6, new end mills.

Figure 2.7: Broken roughing end mill with evidence of thermal degradation.

The dull tool shows worn flute edges that appear blunt and smooth. This visual signature aligns with flank wear and edge rounding often seen during tool aging, particularly in difficult-to-machine materials such as coated superalloys. The absence of clear cutting edges suggests that this tool was used after it exceeded its effective cutting life. Using a dull tool can amplify heat buildup and chatter, leading to more catastrophic forms of breakage

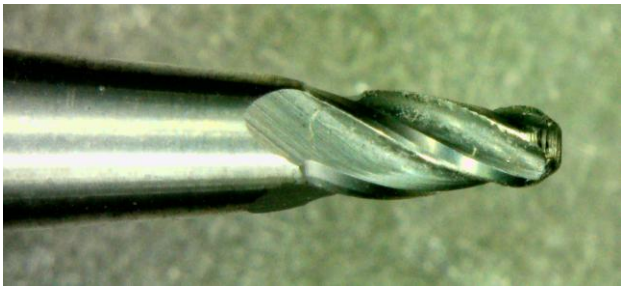

Figure 2.8: Worn roughing end mill with edge dulling.

The shattered example has sharp fractured surfaces and a large portion of the tool missing. This type of failure is typical of mechanical overload or vibrational instability and may have been caused by several suboptimal cutting parameters resulting in excessive force against the end mill during operation. Shattering failures often occur abruptly and without warning signs seen in gradual wear modes.

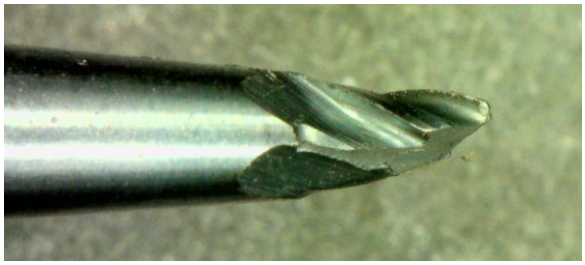

Figure 2.9: Catastrophically fractured roughing end mill.

A similar photograph analysis was performed for the finishing end mills, which are used to machine the deeper, narrower portion of the hole which is inaccessible to the roughing tool. These tools are referred to as finishing tools, however they do not re-machine the portion of the hole milled by the roughing tool, as a conventional finishing tool would. The finishing tools were observed to suffer from the same three failure types, though with different frequencies for each failure mode.

As with the larger tools, two new finishing tools were documented. Figure 2.10 shows a new finishing end mill with a sharp tip. Rotated 90°, Figure 2.11 presents a rounded appearance, showcasing the two flutes meeting at the center axis of the tool. Comparing the sharpness of the tip and flutes in these photographs emphasizes the failure modes displayed in further photos.

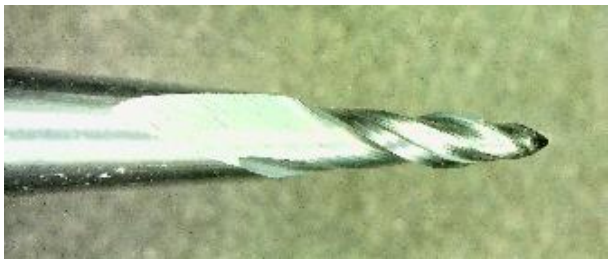

Figure 2.10: New finishing end mill showing sharp tip geometry.

Figure 2.11: New finishing end mill rotated 90° to display flute convergence.

The melted finishing tool shows evidence of thermal degradation concentrated around the tip of the tool. This rounded tip exceeds the profile of the taper in the tool, confirming melting. Of the observed tools, this failure type is far less common in the finishing tools compared to the roughing tools.

Figure 2.12: Broken finishing end mill with evidence of thermal degradation.

The failure in Figure 2.13 is more difficult to see than the other failure modes because it is less drastic in terms of material removed or deformed on the tool. The failure in this tool is an optimal failure, because the tool has been used for its effective life, without being over-used or having the effective life cut short.

Figure 2.13: Worn finishing end mill with edge dulling.

The shattered finishing tool, much like its roughing counterpart, displays abrupt fracture, which may have been caused by several process parameters. The smaller diameter and higher aspect ratio make these tools especially vulnerable to brittle failure. Within the sample of broken finishing tools collected, most of the failures were characterized as shattering.

Figure 2.14: Catastrophically fractured finishing end mill.

These photographs not only illustrate distinct breakage modes but also highlight the visual differences in wear and failure between the roughing and finishing tools. While visual inspection alone cannot definitively determine all failure cases, it is invaluable for preliminary classification and for flagging tools whose failure signatures may correlate with machining conditions, hole geometry, or process variations identified in the later statistical analysis of this thesis.

2.3.2 Post-Failure Tool Length Analysis

To gain further insight into the mechanisms and severity of tool breakage events, all photographed tools were measured after failure. Because the tools were collected from a recycling container, their starting lengths were unknown. However, measurements of unused tools were taken to estimate baseline lengths, allowing for approximate comparisons. To reduce measurement variation and ensure consistent alignment, a custom 3D-printed jig was designed to repeatably hold the tool against a pair of calipers.

Figure 2.15 presents a histogram of the post-failure lengths of all roughing tools photographed. Although the exact starting length of each tool is unknown, a distribution of new tool lengths was used to estimate a nominal baseline. For roughing tools, the average new tool length was 1.5027 inches, with a standard deviation of 0.00218 inches. When a RoboDrill flags a tool as broken, it checks if the tool is within 0.008 inches of the starting length. The histogram shows a strong leftward skew, with the most frequent tool breakage bin being around eight thousandths of an inch of the average new tool length. This pattern suggests that the roughing tools are failing due to standard wear and not breakage.

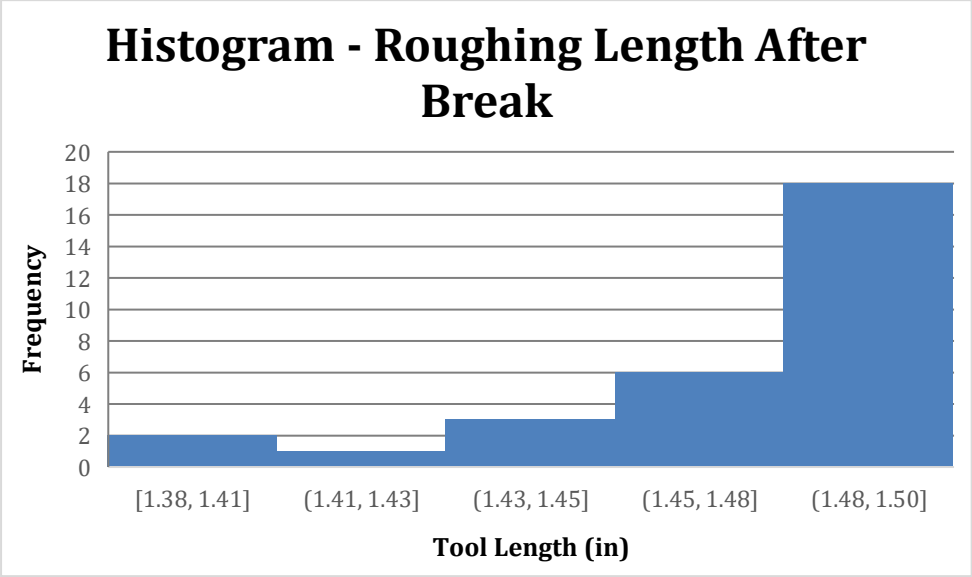

Figure 2.15: Histogram of tool lengths for broken roughing end mills.

This observation from the histogram is reinforced by the breakdown of tool failure frequency presented in Figure 2.16. Here, most roughing tools were classified as having failed by dulling, followed by melting, shattering, and a small percentage that appeared visually new. While the highest frequency of failures were due to dulling, there were still a large percentage of other failure modes. In an ideal case, all the tools would fail due to dulling rather than failure modes that cut their life short, like shattering, or extending them too long, like melting.

The appearance of tools that look new at the time of disposal may seem noteworthy, because they appear to be tools that are discarded prematurely. However, observation of the RoboDrill operators showed that operators dispose of tools due to caution in ambiguous situations, such as if the tool accidentally hits the ceiling of the buffer container when placed, or if the tool does not sit correctly in the heat shrink holder.

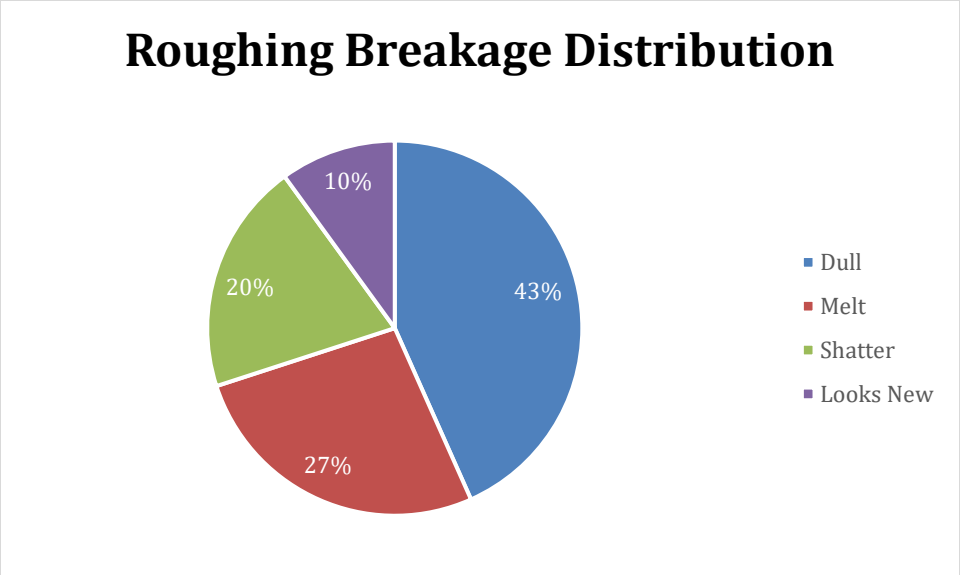

Figure 2.16: Pie chart of breakage types for broken roughing end mills.

The results for finishing tools, shown in Figure 2.17 and Figure 2.18 paint a different picture compared to roughing tools. The average measured length of new finishing tools was 1.5000 inches, with a standard deviation of 0.00202 inches. Figure 2.17 shows a bimodal histogram of tool lengths following failure. One cluster of tools is grouped near the expected failure length at the far right of the histogram, while the second cluster is significantly lower in length. At first glance this may suggest the balanced existence of dulling and melting or shattering as the main failure modes, but the greater number of tools distributed in the lower range of lengths indicates a strong presence of catastrophic breakage.

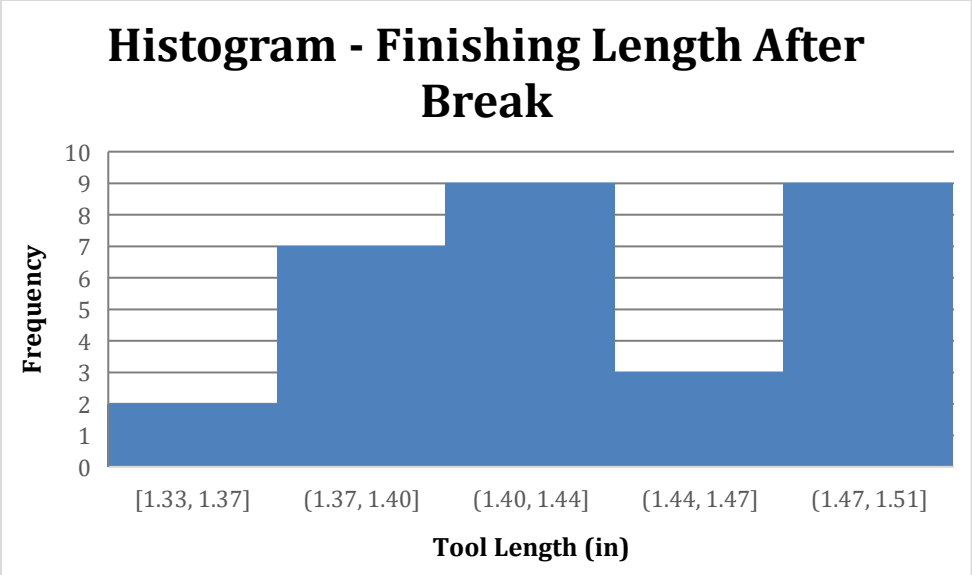

Figure 2.17: Histogram of tool lengths for broken finishing end mills.

This interpretation is supported by the pie chart in Figure 2.18, which shows that shattering accounts for approximately 73% of all failures for the random selection of finishing tools analyzed. It is interesting to note that the location where the tool shatters is inconsistent, with some tools shattering near the tip and others shattering much further up the tool (Appendix A has the measured lengths of all the tools with their images for reference). The two other minor categories of breakage are tools that melt and those that appear visually new. Interestingly, tools that are visually indistinguishable from new tools were more frequent than those that melted, contrary to the pattern observed in the roughing tools.

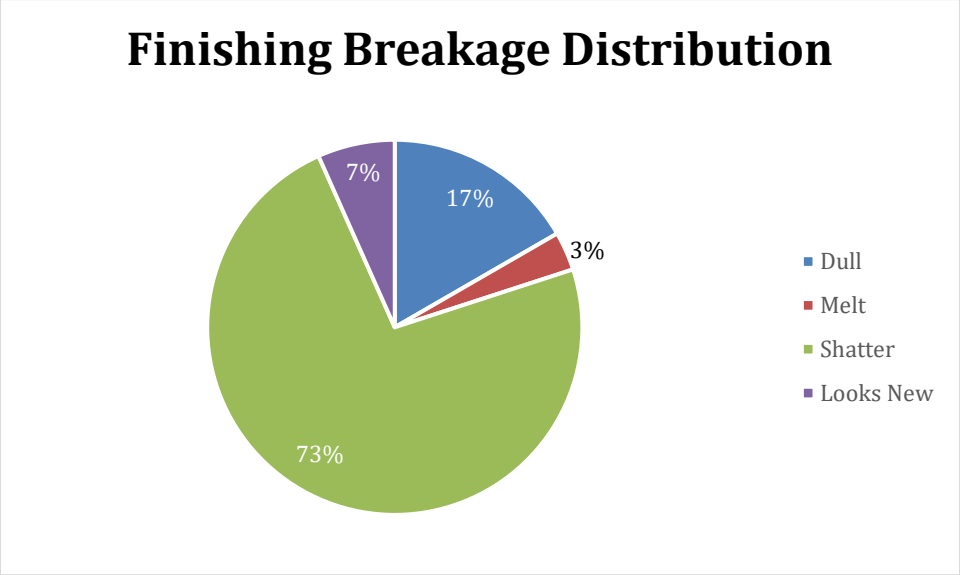

Figure 2.18: Pie chart of breakage types for broken finishing end mills.

These results suggest a meaningful difference in failure characteristics between roughing and finishing tools. The dominance of dulling and melting in roughing tools indicates that extended tool life may be achieved through better thermal management and optimized cutting parameters. In contrast, the frequent shattering of finishing tools suggests the need for a more extreme reworking of cutting path.

This page was intentionally left blank

Chapter 3 Exploratory Analysis of Tool Breakage Trends

3.1 Introduction and Dataset Description

This chapter expands the investigation of tool failures by moving from physical examination of broken tools to the analysis of production data collected over six months of operation. The goal is to characterize the frequency and distribution of tool breakages across the manufacturing process to statistically evaluate whether certain process variables are associated with increased tool breakage. Building on the findings of Chapter 2 which identified the dominant failure modes, this chapter aims to establish more context for tool breakages within the process.

This analysis was prioritized as a critical next step to determine whether tool failures were related to specific machines, rows, or hole features, or if most breakages were due to general process conditions. Understanding these patterns was essential for identifying variables that behaved consistently which allowed for meaningful experiments aimed at improving tool life. Furthermore, this analysis provided an opportunity to uncover process issues resulting in certain holes causing significantly more tools to break than other holes.

The dataset in this chapter comprises six months of production logs from eight RoboDrills. Each log contains the cycle time for the part broken up into the cycle time for each row. The logs also have the runout of each tool in the machine as recorded when the tool was first placed in the machine. The main portion of each log is a list where each entry corresponds to a tool break. Each entry has the tool type, row number, and hole number. Table 3.1 has a list of every row of holes machined into the turbine blade, alongside an abbreviated name which may be used in future figures. Within each machined row, every hole is slightly different due to the complex curvature of the turbine blade, however there are two generalizable cross-sectional shapes that the holes can be categorized into: circles and rectangles. The cross-sectional profiles of the holes are not perfect circles nor perfect rectangles; however, this nomenclature will be used to identify each shape. These shapes were optimized by a design team, and Figure 3.1 shows an example of each type of hole shape.

Table 3.1: All rows machined into the turbine blade with corresponding hole shapes and number of holes.

Row Name	Row Abbreviation	Number of Holes	Hole Profiles
Platform A	Plat A	3	Rectangle
Platform B	Plat B	12	Circle
Platform C	Plat C	22	Circle & Rectangle
Platform D	Plat D	3	Circle
Platform E	Plat E	9	Circle
Platform F	Plat F	10	Rectangle
Stag Row 1	Stag R1	23	Circle
Pressure Side Row 2	PS R2	23	Circle
Pressure Side Row 3	PS R3	30	Rectangle
Pressure Side Row 4	PS R4	35	Rectangle
Pressure Side Row 5	PS R5	26	Rectangle
Suction Side Row 2	SS R2	23	Circle
Suction Side Row 3	SS R3	23	Circle
Suction Side Row 4	SS R4	50	Rectangle
Slashface Pressure Side	Slash PS	17	Circle
Slashface Suction Side	Slash SS	13	Circle
Trailing Edge	TE	71	Circle
Tip Row 1	Tip R1	28	Circle
Tip Rail	Tip Rail	13	Circle
Tip Cap	Tip Cap	28	Circle

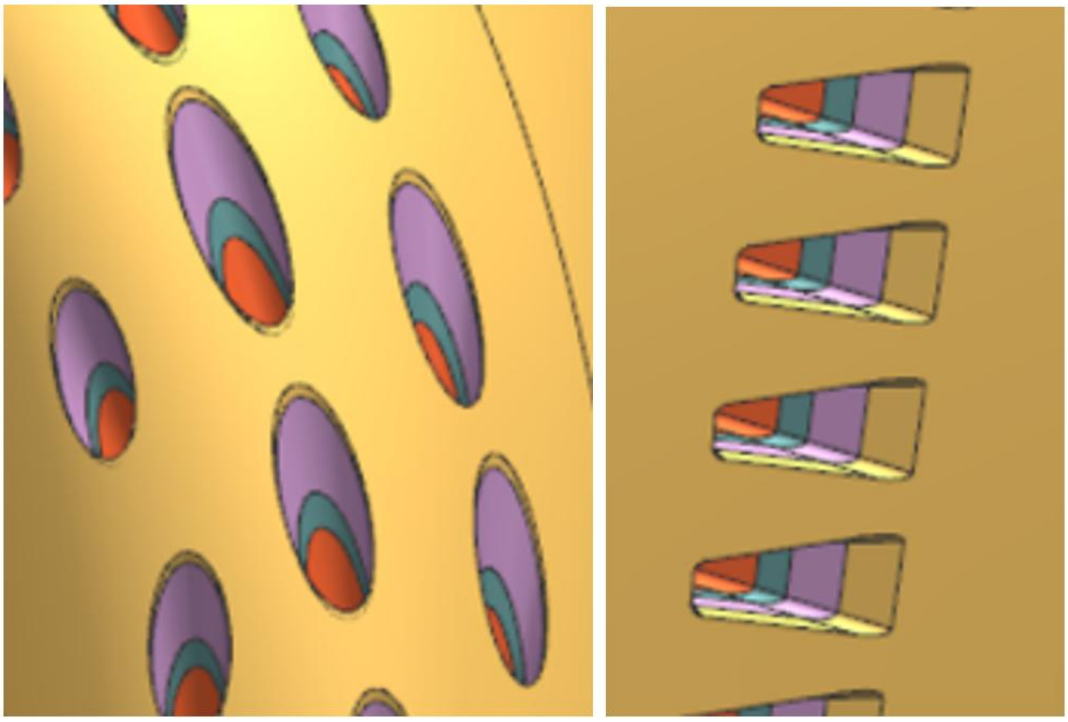

Figure 3.1: Two different diffuser hole shapes: circle (left) and rectangle (right).

Due to the nature of the production process, certain limitations were present. Tool replacement during operation was handled by operators, and therefore the type of tool failure was not obtained. As mentioned in Chapter 1, the tools are only measured when they are first put into the RoboDrill. To determine a break, the machine uses a laser and checks if the tool is within 0.008 inches of the original recorded length. Because of this, no data about the tool is recorded when a break occurs.

The findings of this chapter served two key purposes. First, they provided actionable insight into which aspects of the process are contributing most to tool failure, allowing for the focus of the project to narrow to areas of high breakage rates. Second, they defined the scope of subsequent chapters by identifying collections of holes that behave similarly.

3.2 Frequency and Distribution of Breakages

To better understand patterns of tool breakage, a dashboard was developed in Python to visualize six months of tool failure data. The initial framework for this dashboard was previously developed by a GE Vernova employee, but it was unfinished and required debugging and improvement to produce meaningful results. The most meaningful graphs are highlighted in this section, and the rest can be found in Appendix B.

Figure 3.2 presents a bar chart of the total number of tools broken by row, with each bar segmented by tool type. The chart reveals several rows which have disproportionately high tool breakages, namely Suction Side Row 2, Suction Side Row 3, Stag Row 1, and Pressure Side

Row 2. Comparing these rows to Table 3.1 which summarizes row geometries, it is noted that all four of these rows have circular profiles. Also, all four of these rows are near one another on the leading edge of the blade. This correlation suggests that hole geometry or blade location may be a significant factor influencing tool failure. Furthermore, while rows with fewer holes would intuitively be expected to cause fewer breaks, this trend is not consistent. The elevated failure rates seen in rows with comparable holes indicate that geometry and other process variables are likely greatly influencing tool life.

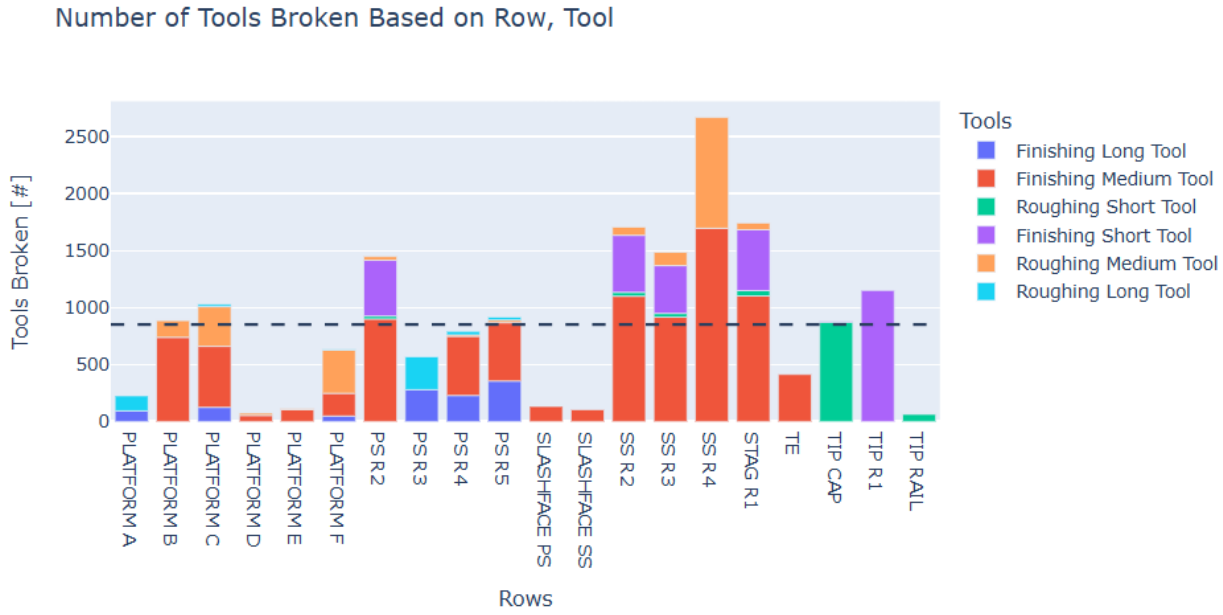

Figure 3.2: Bar chart of total tool breakage by row, segmented by tool type.

To evaluate the potential influence of tool concentricity on these failures, Figure 3.3 illustrates the average runout for each tool type. As expected, longer tools exhibit greater average runout due to increased deflection and geometric sensitivity. The longest finishing tools show a marked increase in runout compared to their shorter counterparts. It is important to note that runout is only measured when a new tool is mounted in the machine. In-process runout is not captured due to the time cost of measuring after each operation.

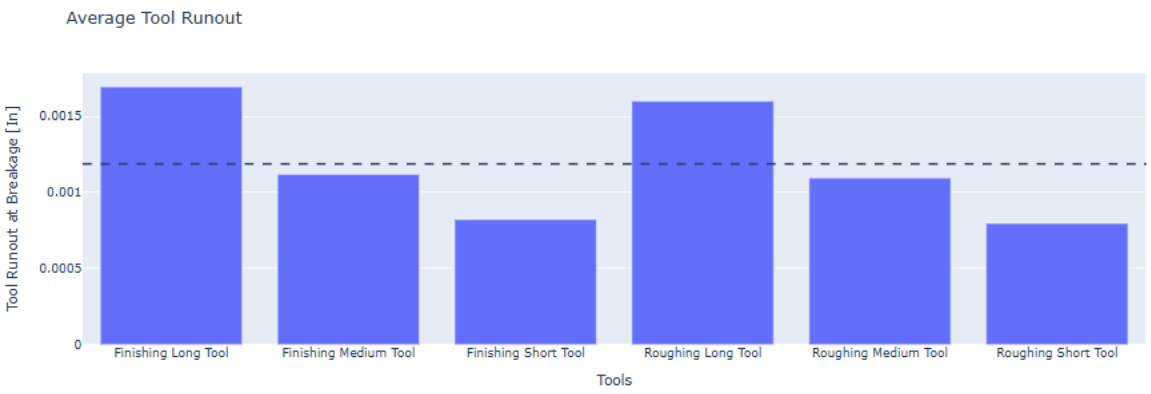

Figure 3.3: Bar chart of average runout by tool type.

The distribution of broken tools by type, presented in Figure 3.4, shows a significant concentration of failures by the medium length finishing tool. This tool type alone accounts for 53% of all recorded breakages over six months of data. Further investigation into this revealed that this tool is by far the most frequently used. When combined, all the finishing tools represent approximately 78% of all failures. This information narrows the focus of this study to the smaller diameter finishing tools because improvements in that area have the greatest potential impact on the process.

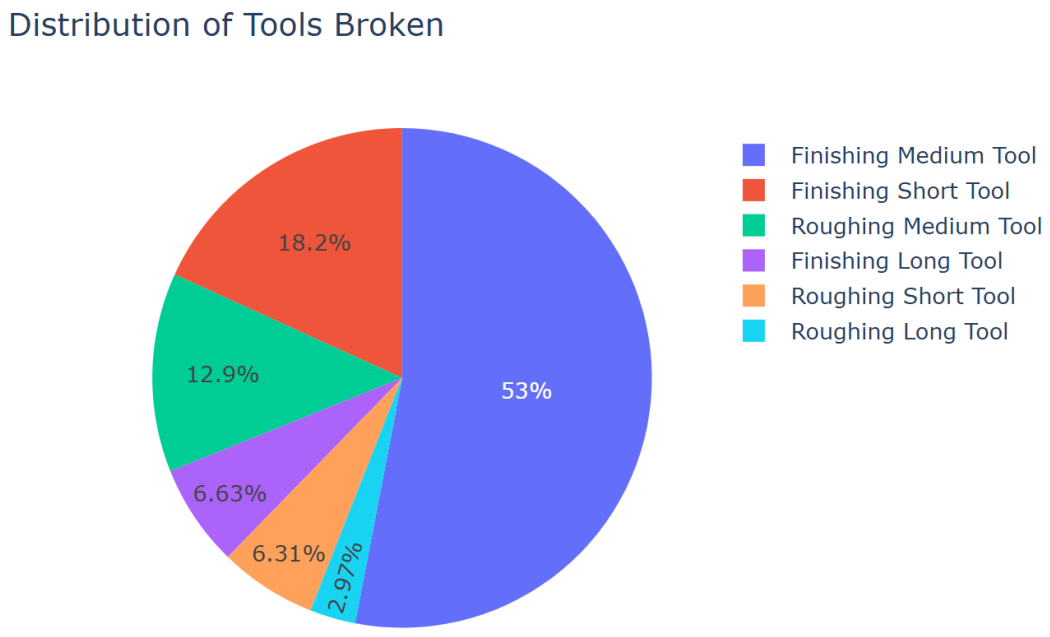

Figure 3.4: Pie chart showing tool breakage distribution by tool type.

To further refine the understanding of failure patterns, Figure 3.5, much like Figure 3.2, once again plots tool breakage across rows, but this time separates each bar by hole number. This visualization uncovered two holes with significantly elevated failure rates compared to others. This chart sparked an investigation into the programming of Platform B Hole 4 and Platform C Hole 11. This chart shows separate hole entries for roughing and finishing operations, and therefore it is known that both problematic holes are causing the finishing tool to break.

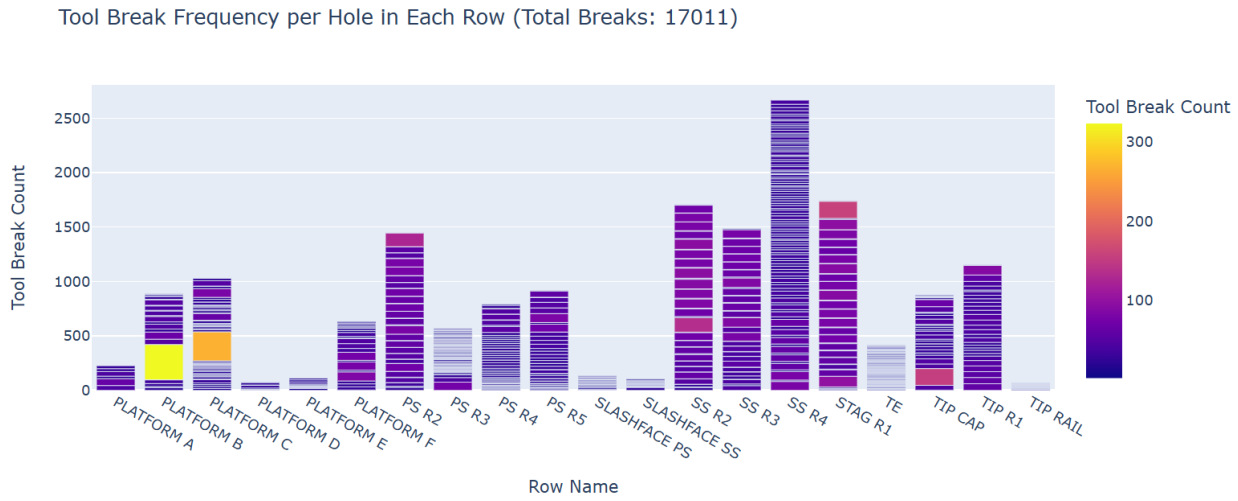

Figure 3.5: Bar chart of total tool breakage by row, segmented by hole.

It was discovered that both holes had significant programming errors. For CAM programming, a toolpath is provided to the RoboDrills. This path is a helix shape that the RoboDrills follow to machine a hole. In each toolpath, the tip of the tool follows the path; this results in the finishing tool requiring a larger diameter path to match the outer surface of the hole cut by the roughing tool. For Platform C Hole 11, the initial program lacked overlap between the roughing and finishing operations. Figure 3.6 illustrates the original and corrected toolpaths. Because of this gap between the toolpaths for each tool, the machine would plunge the finishing tool directly into solid metal before attempting to cut, shattering the tool. The correct toolpath, shown on the right, has an overlap between the roughing and finishing path so that the finishing tool would start spinning a bit before it encountered the metal. Additionally, because tools are not remeasured after each hole, it is never known where the roughing pass ended exactly. The bottom face of the hole could be within eight thousandths of an inch of where it is programmed to be because the tool is not flagged as broken until it wears past that point. Because of this, the overlap between the roughing and finishing pass needs to be at least 0.008 inches. This issue had gone unnoticed in production because the RoboDrill was programmed to skip a hole after two consecutive tool failures. This prevented further failures but masked the underlying problem. Once identified, the program was updated to properly overlap the two paths.

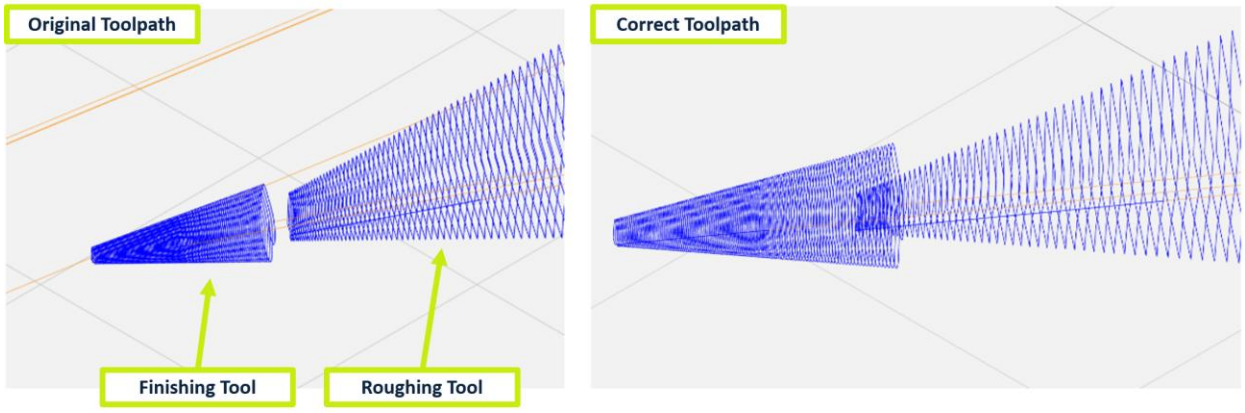

Figure 3.6: CAM toolpath comparison for Platform C Hole 11.

A similar programming oversight was found in Platform B Hole 4, where dynamic feed reduction near the bottom of the hole was not enabled. As the tapered helical toolpath narrows in diameter, the feed rate is supposed to decrease to ensure accuracy and to reduce cutting forces. This issue was also updated in the CAM file.

Besides the two holes with extreme breakage rates, other holes exhibit disproportionate breakage rates, such as those at the top of the Pressure Side Row 2 bar and the Stag Row 1 bar, and at the bottom of the Suction Side Row 4 bar. These breakage rates were determined to be influenced by the complex curvature of the blade surface. These holes were located on very curved surfaces, requiring modified entry angles and toolpaths.

The insights from these charts demonstrate the importance of data visualization in identifying both systematic trends and specific process deficiencies. The Python dashboard not only enabled these discoveries but also facilitated immediate corrective actions that improved tool breakage. The findings from this section also narrow the focus of the project to finishing tools which further chapters will focus on.

3.3 Statistical Analysis to Identify Significant Factors

3.3.1 Between-Machine Significance

To assess whether significant differences exist in tool breakage rates across the eight Fanuc RoboDrill machines in operation. One-way analysis of variance (ANOVA) was performed on a historical dataset of tools broken per part. This is the same dataset that the Python dashboard referenced. Prior to applying this technique, it was essential to verify that the distribution of tool failures per part approximately followed a normal distribution. Figure 3.7 shows a histogram of tools broken per part, which visually appears symmetrical and bell-shaped. To confirm normality more rigorously, a Q-Q plot was generated. This can be seen in Figure 3.8. In this plot the dots

are the dataset, and the line is a perfectly normal distribution. The dataset closely follows a normal distribution, which supports the use of ANOVA. It is important to note that machines NL1030 and NL1031 have fewer than ten historical data logs and therefore they were omitted from this analysis.

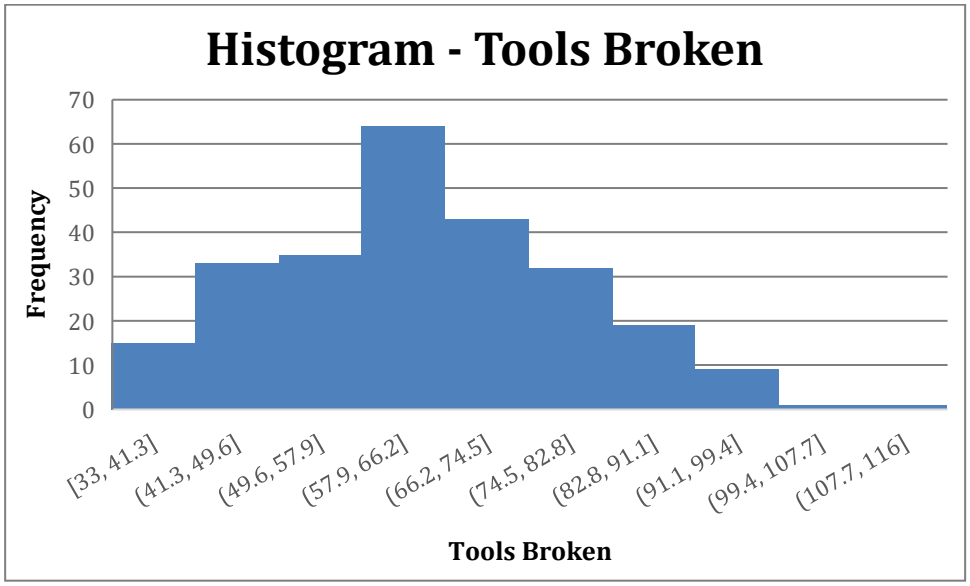

Figure 3.7: Histogram of tools broken per part.

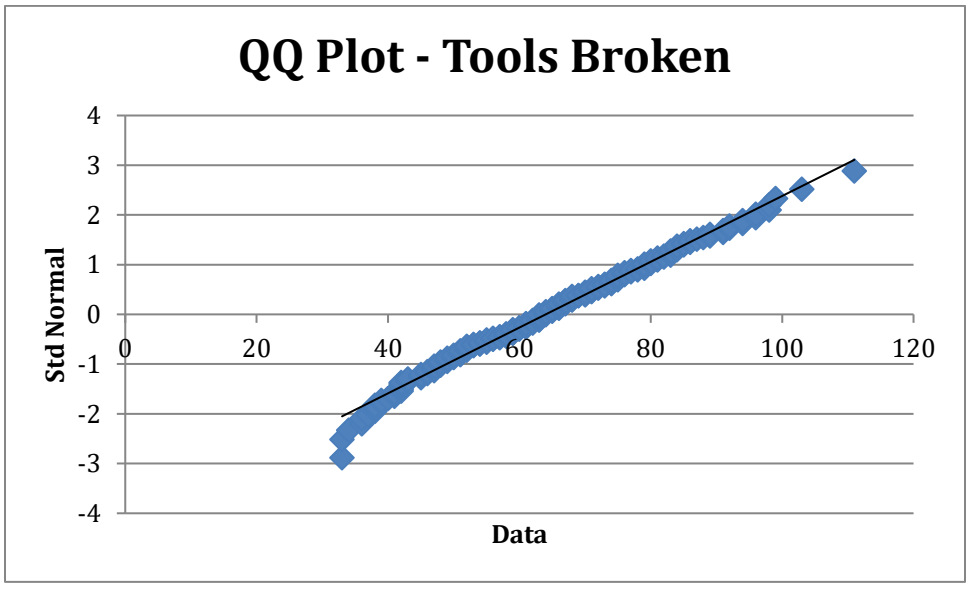

Figure 3.8: Q-Q plot of tools broken per part. This plot implies normal behavior because of the linearity of the data.

ANOVA, or Analysis of Variance, is a statistical method used to determine whether there are statistically significant differences between the means of three or more independent groups.

In this context, it tests the null hypothesis that all machines produce parts with the same mean tool breakage rate. A significant ANOVA result suggests that at least one machine's mean differs from the others, though it does not identify which pairs of machines differ or the direction of the difference. In the ANOVA analysis, a p-value of 8.2E-10 was calculated, suggesting a high level of statistical significance. The calculated ANOVA table can be found in Appendix C. Traditionally, the null hypothesis is rejected when the p-value is smaller than 0.05, meaning that there is a 95% confidence level that the results are not because of randomness.

To pinpoint which machines differ from one another, a Tukey Honest Significant Difference (HSD) post-hoc test was conducted following the ANOVA. Tukey HSD performs pairwise comparisons between all possible combinations of variable pairs. This test outputs p-values for each pair of machines compared. Unlike ANOVA which only identifies a difference, the Tukey HSD test maps out the relationship between machines.

Table 3.2 summarizes the results of this analysis. Each row represents one machine and lists its mean number of tools broken per part. The table also shows how often each machine was found to be statistically different from other machines in the Tukey HSD test, listed as significance frequency. A 0.05 p-value threshold was used in this analysis. For significance frequency, conditional formatting was used where the least significant machine is green and the most significant is red. Additionally, the mean tool break values were conditionally formatted with red as the highest value and white as the lowest. From this table, it is seen that machine NL1025 has the lowest average tool breakage rate and NL1024 has the highest. Because of this, these two machines were flagged as the most statistically significant compared to the others. Machine NL1033 was found to be the most average performing machine, with the least amount of statistical difference from all the other machines. While future tests will be done on a RoboDrill that is functional but not yet in operation as the factory expands, it is important to have done this analysis as groundwork for determining which machine to do testing on to provide the most meaningful results. Results from tests on NL1033 will be the most broadly applicable to all machines if testing cannot be done on all of them.

Table 3.2: Tukey HSD significance counts for each machine and mean tool breakage per part. Significance frequency is formatted with red as the most significant and green as the least significant. Mean is formatted with red as the highest value and white as the lowest.

Group	*significance frequency*	*mean*
NL 1023	2	58.4
NL 1024	3	72.6
NL 1025	4	41.9
NL 1032	2	52.8
NL 1033	1	66.3
NL 1034	2	67.6

To investigate possible root causes, historical maintenance logs were reviewed for all machines. Surprisingly, no clear correlations emerged between recorded maintenance events and tool breakage rates. However, an observation on the factory floor revealed a critical issue with NL1024 that was not documented in the maintenance logs. As seen in Figure 3.9, a small note affixed to the machine instructed operators to avoid using 100% rapid traverse speeds. Rapid traverse refers to the machine's high-speed, non-cutting movements between holes or tool changes. An engineer revealed that at full speed the rotary table would fault the machine. The rotary table does not move during hole milling, it only moves between holes to align the part with the spindle, and therefore all its movements are in rapid traverse mode.

Figure 3.9: A note on NL1024 hiding the 100% rapid traverse override button.

Further discussions with engineers confirmed that this limitation existed since the machine's installation and was never formally addressed. This undocumented hardware fault means that NL1024 must operate at reduced rapid traverse speeds, and it can be assumed that the imprecise rotary table is decreasing tool life. This discovery highlights the value of Gemba walks, where engineers visit the production environment and directly observe the process and

interact with the operators. Without this engagement, this critical information would have remained invisible in the data.

3.3.2 Between-Row Significance

While the previous section examined variability in tool breakage rates between machines, this section focuses on the variability between rows on the turbine blade. Using the number of broken tools per row in this analysis is misleading because each row contains a different number of holes. To normalize the data, the total number of tools broken per row was divided by the total number of holes milled in that row. This metric provides a fair basis for comparing rows, and the inverse of this number serves as an estimate for tool life in that row.

Upon graphing this normalized data, the data was shown to be exponentially distributed as opposed to normally distributed. This can be seen in Figure 3.10. This violates a key assumption of the ANOVA test, which requires normally distributed data. To address this, a Kruskal-Wallis test was performed instead. The Kruskal-Wallis test is a non-parametric alternative to ANOVA that works by assessing whether the median across groups is different as opposed to means. Similar to one-way ANOVA, the goal of this test is to provide a statistical confidence level that groups originated from the same statistical distribution.

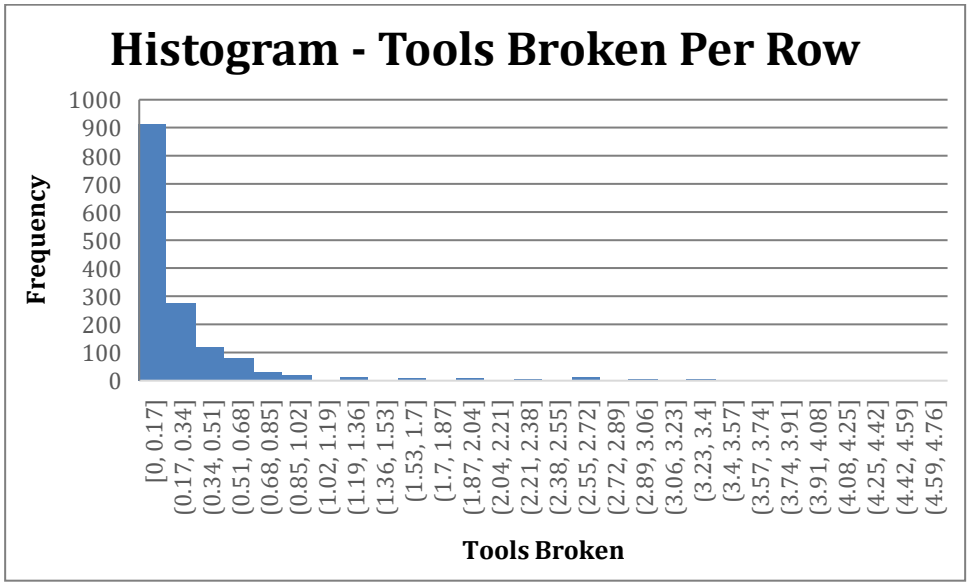

Figure 3.10: Histogram of tools broken per row, normalized by number of holes per row. Each bin contains data, although difficult to see due to the exponential distribution.

The Kruskal-Wallis test output a p-value of 5.25E-14, strongly rejecting the null hypothesis that all rows behave the same. To further investigate the difference in rows, a DUNN's test was employed. Like Tukey's test for ANOVA, DUNN's test compares all possible pairs of groups while adjusting for multiple comparisons. Importantly, the DUNN's test does not require the data to be normally distributed. Table 3.3 summarizes the findings from this analysis

by showing the mean normalized tool breakage value per row and the frequency that each row was identified as significantly different from the other rows in the DUNN's test. The results from the DUNN's test on machine 1023 can be found in Appendix C. To visualize these results better, conditional formatting was utilized. Rows with higher tool breakage rates are shaded in red with lower values being white. For the DUNN significance, rows that were significantly different were shaded white and those that were less frequently significant were shaded green.

Table 3.3: DUNN significance count and mean tool breakage per row divided by number of holes in row. Significance frequency is formatted with green as the least significant. Tools broken is formatted with red as the highest value.

group	Average Significance Frequency:	*Tools Broken:*
TIP RAIL	6.50	0.018
SS R3	4.33	0.266
SS R2	5.83	0.280
STAG R1	6.00	0.291
PS R2	4.67	0.237
TIP R1	1.17	0.144
SS R4	2.17	0.177
PS R3	1.33	0.089
PS R4	1.50	0.064
PLAT A	0.83	0.222
PLAT B	5.00	0.244
PLAT C	0.83	0.151
PLAT D	3.33	0.072
PLAT E	4.83	0.035
PLAT F	1.67	0.203
SLASH SS	4.33	0.031
SLASH PS	4.83	0.027
PS R5	0.00	0.107
TE	4.83	0.015
TIP CAP	0.00	0.108

This analysis once again highlighted that Suction Side Row 3, Suction Side Row 2, Stag Row 1, and Pressure Side Row 2 are problematic. Their increased significance proves that they disproportionately contribute to tool breakage, warranting further investigation.

3.3.3 Hole Geometry Significance

This analysis seeks to determine whether circular and rectangular holes, seen in Figure 3.1, exhibit distinct tool breakage behaviors. Because rows vary in their specific hole geometries,

a subset of similar rows was selected for each hole type to minimize variation within each group. For circular holes, Suction Side Row 3, Suction Side Row 2, Stag Row 1, and Pressure Side Row 2 were selected because they all feature similar hole geometries and all exhibit high tool breakage rates. For rectangular holes, Suction Side Row 4, Pressure Side Row 3, Pressure Side Row 4, and Pressure Side Row 5 were selected.

To account for the differences in the number of holes across rows, the dataset was normalized by dividing the total number of tools broken per group by the total number of holes in the collective rows. A box plot to visualize this data can be found in Figure 3.11. Initial inspection of the data through Q-Q plots, as seen in Figure 3.12 and Figure 3.13, suggested that both datasets were approximately normally distributed, although slight deviations were observed in the plot for the circular holes. To further validate normality, Shapiro-Wilk and d'Agostino-Pearson tests were performed, both confirming normality at a 95% confidence level.

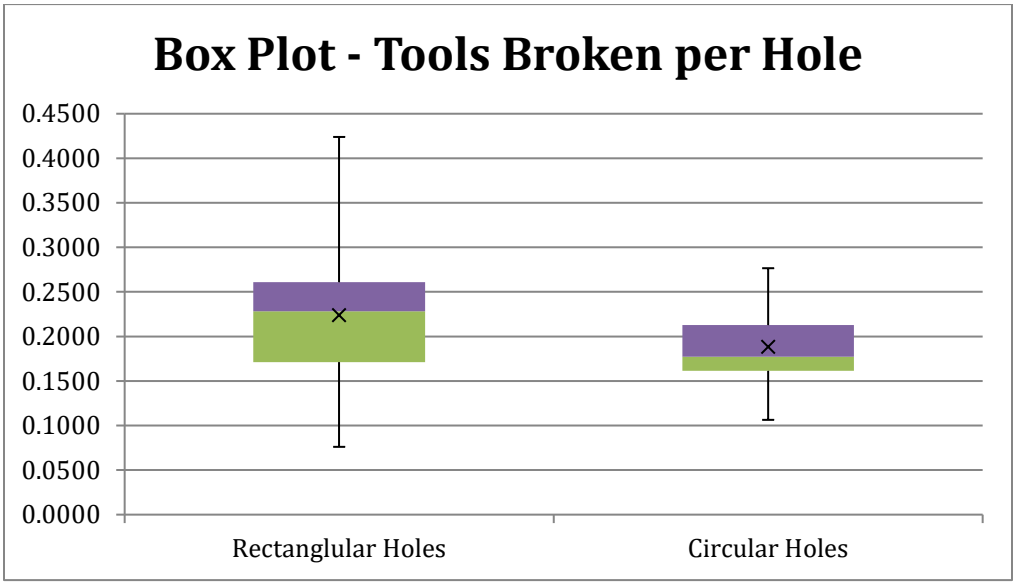

Figure 3.11: Box plot of tools broken by hole, segmented by hole profile and normalized by hole count.

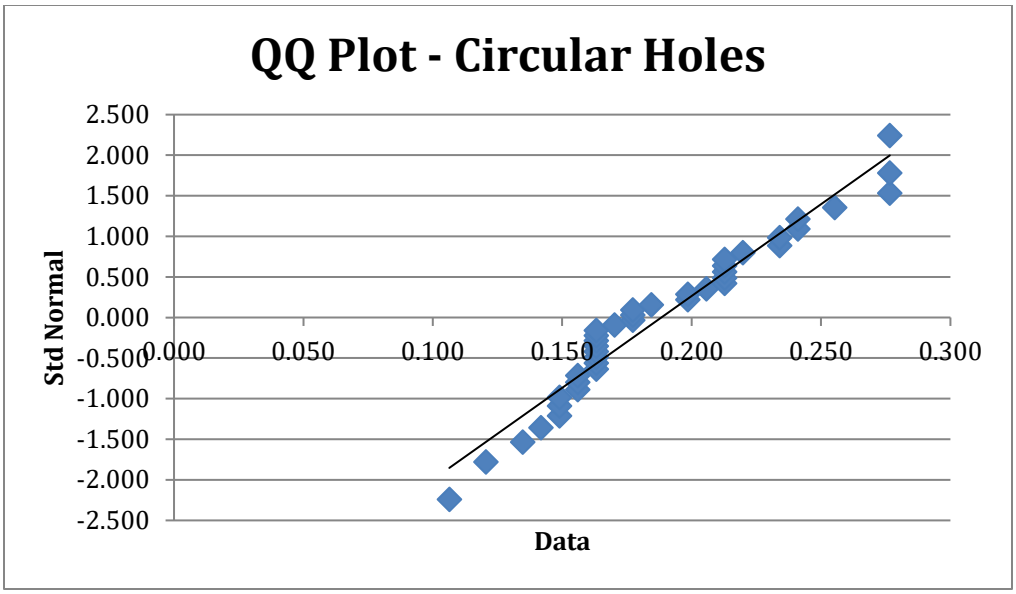

Figure 3.12: Q-Q plot of tools broken per select rows with circular holes. This plot implies normal behavior because of the linearity of the data.

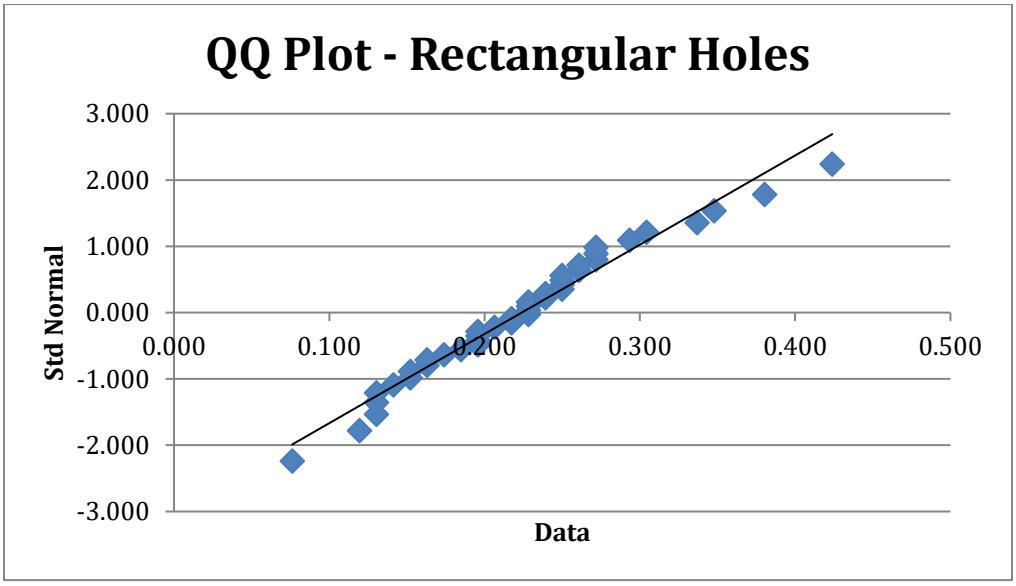

Figure 3.13: Q-Q plot of tools broken per select rows with rectangular holes. This plot implies normal behavior because of the linearity of the data.

With normality established, a two-tailed t-test assuming unequal variances was conducted to assess the significance of tool breakage rates between the two hole profiles. This test resulted in a p-value of 0.0099 which suggests a meaningful difference between the two groups. This finding highlights that future experimentation should focus on either circular or rectangular holes independently to avoid effects from their differences.

Focusing further on circular holes, a one-way ANOVA was performed to evaluate if the selected rows behave similarly. This analysis, found in Table 3.4, produced a p-value of 0.0289 which rejects the hypothesis that the difference in rows is due to randomness. Closer examination of the table revealed Stag Row 1 to be an outlier due to the large mean and variance.

Table 3.4: One-way ANOVA table comparing normalized tool breakage between select rows with circular holes.

DESCRIPTION					Alpha	0.05		
Group	*Count*	*Sum*	*Mean*	*Variance*	*SS*	*Std Err*	*Lower*	*Upper*
SS R3	10	2.826	0.283	0.0106	0.0955	0.0313	0.219	0.346
SS R2	10	2.391	0.239	0.00809	0.0728	0.0313	0.176	0.303
STAG R1	10	3.478	0.348	0.0143	0.129	0.0313	0.284	0.411
PS R2	10	2.174	0.217	0.00630	0.0567	0.0313	0.154	0.281
ANOVA								
Sources	*SS*	*df*	*MS*	*F*	*P value*	*Eta-sq*	*RMSSE*	*Omega Sq*
Between Groups	0.0992	3	0.0331	3.37	0.0289	0.219	0.580	0.151
Within Groups	0.353	36	0.00982					
Total	0.453	39	0.0116					

To assess the circular holes without Stag Row 1, a second ANOVA was performed. This ANOVA can be found in Table 3.5 and produced a p-value of 0.283. This p-value is greater than the set limit of 0.05, and therefore this result suggests that the null-hypothesis that Suction Side Row 2, Suction Side Row 3, and Pressure Side Row 2 have no statistical difference cannot be rejected. This result supports the grouping of these rows for future experiments. By controlling hole type and excluding nuisance rows, the results from future experiments will be more accurate and meaningful.

Table 3.5: One-way ANOVA table comparing normalized tool breakage between select rows with circular holes

DESCRIPTION					Alpha	0.05		
Group	*Count*	*Sum*	*Mean*	*Variance*	*SS*	*Std Err*	*Lower*	*Upper*
SS R3	10	2.826	0.283	0.0106	0.0955	0.0289	0.223	0.342
SS R2	10	2.391	0.239	0.00809	0.0728	0.0289	0.180	0.298
PS R2	10	2.174	0.217	0.00630	0.0567	0.0289	0.158	0.277
ANOVA								
Sources	*SS*	*df*	*MS*	*F*	*P value*	*Eta-sq*	*RMSSE*	*Omega Sq*
Between Groups	0.0221	2	0.0110	1.32	0.283	0.0893	0.364	0.0211
Within Groups	0.225	27	0.00833					
Total	0.247	29	0.00852					

3.3.4 Tool Length Significance

Building upon the findings of section 3.3.3 Hole Geometry Significance, an additional analysis was performed to evaluate the influence of tool length on breakage rates within the selected circular rows. For these rows, the RoboDrill uses a short tool for the first 10 holes and switches to a medium length tool for the remaining 13 holes. Due to this unequal distribution of holes, the dataset was once again normalized by dividing the number of tools broken by the number of holes in the group. This analysis focuses on only the finishing tools because they break the most and are the focus of this study. Including the roughing tools in this analysis would provide a layer of uncertainty in the results.

Following the same analysis as previous sections, the data was first assessed for normality. The Q-Q plots for each tool, seen in Figure 3.14 and Figure 3.15, illustrate that the data is not normally distributed because while both datasets appear close to the line of normality, they exhibit a smooth curve which deviates from it. Both a Shapiro-Wilk test and a d'Agostino-Pearson test confirm the lack of normality.

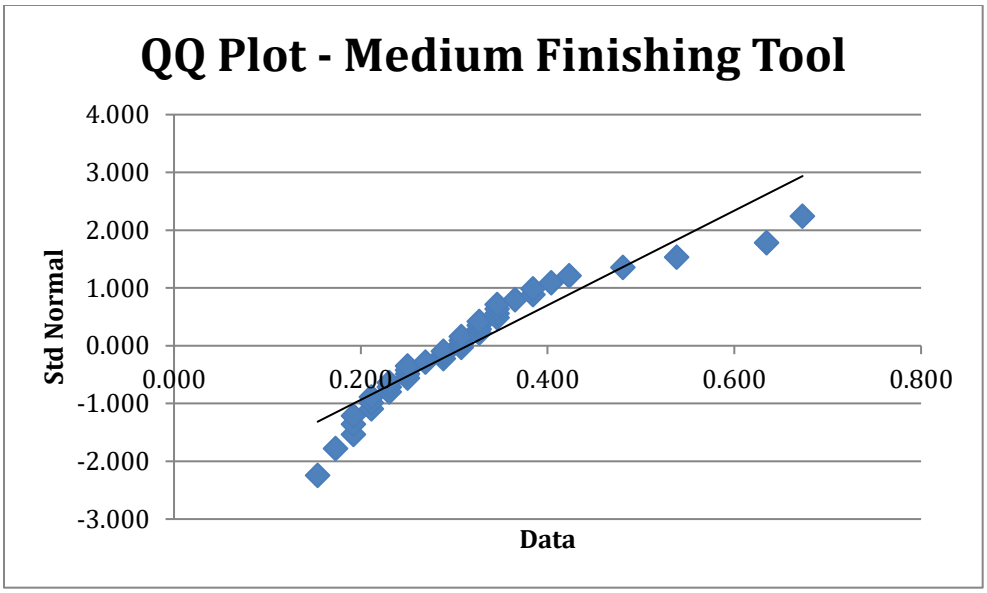

Figure 3.14: Q-Q plot of medium length tools broken per select rows with circular holes. This plot implies non-normal behavior because of the non-linearity of the data.

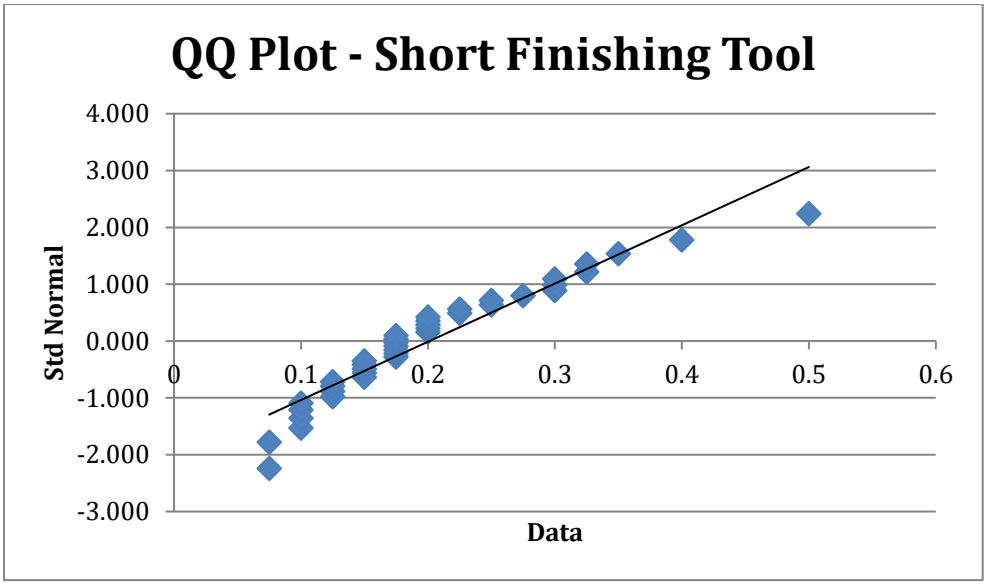

Figure 3.15: Q-Q plot of short length tools broken per select rows with circular holes. This plot implies non-normal behavior because of the non-linearity of the data.

Because the data was not normally distributed, a two-tailed Mann-Whitney U test was selected as an alternative to a t-test. This test yielded a p-value of 5.61E-7, strongly indicating statistical significance between the two tool lengths. Because these tools behave differently, combining them in future experiments would introduce this difference into the experiment in an uncontrolled manner. Future testing should be exclusively performed with one tool length, with the medium-length tool being ideal due to it being used for a larger number of holes on the rows

on interest. Also, as shown in Chapter 2, medium length finishing tools make up 53% of all tool breakages. Focusing on this tool for further experiments therefore maximizes the impact of any progress improvements derived from the research.

Chapter 4 Tool Wear Progression Analysis

4.1 Motivation and Context

The prior chapters of this thesis establish a foundation for understanding patterns of tool failure in the production of cooling holes on turbine blades. This chapter aims to examine how small-diameter carbide end mills degrade over time within the production process.

Currently, the production process relies on a wear threshold of 0.008 inches to identify broken tools. This threshold is implemented within the RoboDrill system, which measures tool length after each hole using a laser. Instead of fully measuring the tool, the RoboDrill saves time by moving the tool to 0.008 inches below the laser and checking if the laser is blocked. If the laser line is broken by the tool, it has not worn by 0.008 inches, and it is used again. If the laser is not blocked, the tool is flagged as broken and the RoboDrill uses a duplicate of that tool loaded in the machine. When all duplicates of one tool are broken, the machine opens and waits for an operator to replace the tools. While this approach is effective in determining tool breakage at a macro scale, it does not provide insight into the tool's wear leading up to breakage.

The hole-by-hole wear tracking analysis presented in this chapter aims to fill the gap in the current tool breakage detection protocol. By systematically photographing and measuring tool length after every hole milled by a tool, this experiment offers a visualization of wear progression under process conditions. This analysis looks at how tools wear while also looking into pre-breakage indicators. A more in-depth analysis of pre-breakage indicators can be found in the partner thesis on this project, written by Luke Placzek [8].

4.2 Experimental Setup: Hole-by-Hole Wear Tracking

To investigate the progression of tool wear leading up to breakage, a controlled study was performed on production turbine blades. The experiment prioritized minimal disruption to the manufacturing process while enabling tracking of tool length after each machining operation.

The test utilized the existing RoboDrills and production parts on the factory floor. After each hole was machined, the RoboDrill was paused. Manual G-code commands were entered to initiate a tool length measurement using the onboard laser. This process ensured that each individual hole's effect on the tool wear could be captured, allowing for a wear curve to be plotted.

The RoboDrill was programmed to spin the spindle at 3000 RPM during each measurement cycle. This practice was implemented with the intention of ejecting residual coolant from the tool and avoiding coolant from accumulating in a way that might interfere with the laser measurement. Preliminary testing across various spindle speeds confirmed that measurements at low RPMs were stable and accurate, while excessively high RPMs occasionally cause the RoboDrill to fail to record the length or runout of the tool. The decision to set the spindle speed to 3000 RPM was also guided by the shop floor manager.

4.3 Wear Progression Results

The primary output of the hole-by-hole testing was a set of detailed wear progression curves, which track the change in length of a tool between holes in a row. This section presents the results for both the finishing and roughing tools on both rectangle-profile holes and circle-profile holes.

4.3.1 Medium Length Finishing Tool Wear on Stag Row 1

The first set of experiments focused on Stag R1 using the medium length finishing tool. For this test, four tools were run until breakage, with tool length measured after each hole. Figure 4.1 shows the resulting tool wear curves for each tool, where the x-axis represents the cumulative number of holes milled, and the y-axis indicates the change in measured tool length. Each curve terminates with an "X" marker, signaling the final hole successfully milled before catastrophic breakage.

As expected from the historical breakage data, each tool lasted approximately two holes and failed on the third. Importantly, while all tools followed a consistent wear curve, the point of failure varied. Despite the wear curve being reproduceable, there is no obvious pre-failure indicator shown from tool length.

Only four tools were tested in this experiment due to the labor-intensive nature of the manual measurement process. It is important to note that this test assumes holes behave similarly even though they are all slightly different to one another. Nevertheless, the consistent wear mechanism up until failure suggests that the holes wear the same amount. Each hole's effect on shattering the tool cannot be concluded.

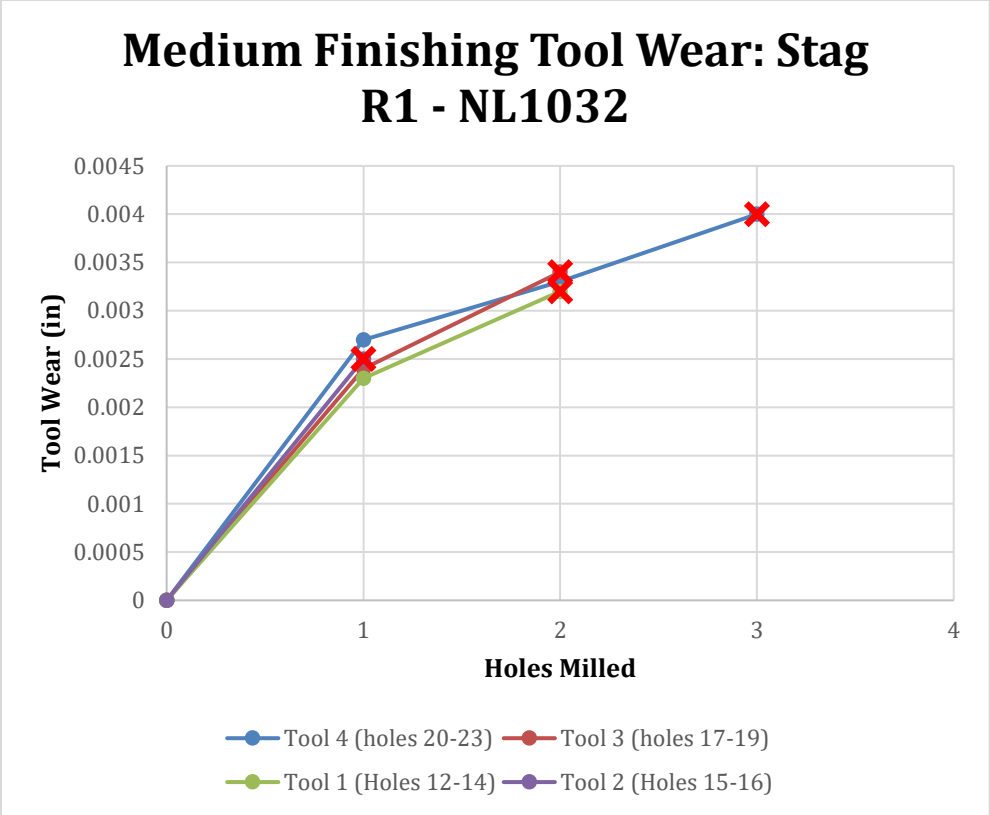

Figure 4.1: Medium length finishing tool wear plotted across holes on Stag Row 1.

4.3.2 Medium Length Finishing Tool Wear on Suction Side Row 4

The second test focused on the same medium length finishing tool but applied it to Suction Side Row 4 which is comprised of rectangular holes and was shown to be significantly more reliable in previous analyses. In this test a single tool was measured after each hole. Unlike the previous test, the tool did not break during this test. Because of this, the test was concluded when the studied row was completed.

As shown in Figure 4.2, after 10 holes the tool only exhibited 0.0013 inches of wear. This is well within the operational limit of 0.008 inches that flags a tool as broken. In comparison, the tools on Stag R1 wore by approximately 0.0025 inches after the first hole milled. This stark contrast reinforces earlier conclusions that the variation between rows plays a dominant role in the wear rates of tools. This also confirms the focus on circular holes as opposed to rectangular holes.

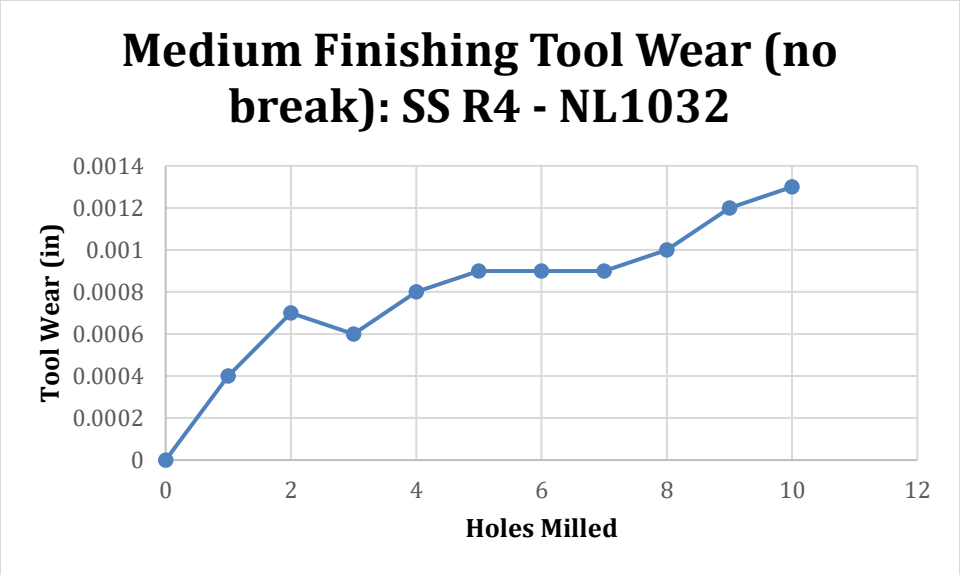

Figure 4.2: Medium length finishing tool wear plotted across holes on Suction Side Row 4. The tool used in this experiment lasted the entire row and therefore the experiment was concluded before it broke.

4.3.3 Medium Length Roughing Tool Wear on Suction Side Row 4

The third wear progression graph, Figure 4.3, tracks the wear of a roughing tool on the same holes as the previous finishing test. This test started three holes earlier, however, and therefore 13 holes are plotted as opposed to 10. The results from this test were informative, however no large conclusions were drawn from it. As expected, the roughing tool did not break and therefore the test was concluded when the studied row was completed.

This graph does follow trends documented in machining literature: namely a steep initial wear stage followed by a linear wear stage. The initial wear is caused by the tip dulling after the first hole. Following the initial wear, the tool behaves as expected, with a small amount of wear after each hole. While no major conclusions were drawn from the graph, this can serve as a reference for future work done by GE Vernova on this project.

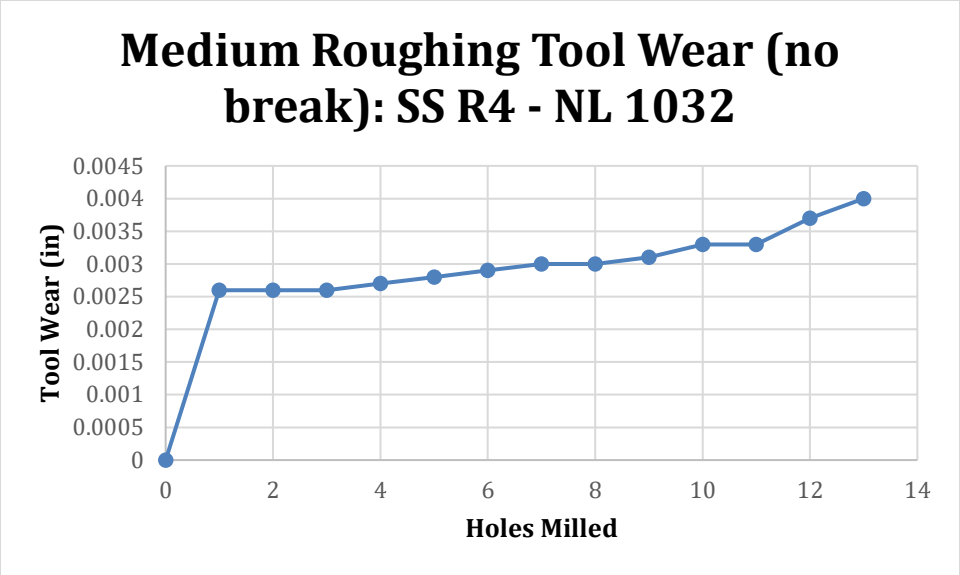

Figure 4.3: Medium length roughing tool wear plotted across holes on Suction Side Row 4. The tool used in this experiment lasted the entire row and therefore the experiment was concluded before it broke.

4.3.4 Roughing Tool Hole Depth Documentation

During the wear testing process, it was discovered that on certain rows the roughing tool did not cut into the base metal and instead only cut though the ceramic coating. This was only happening on rows that had irregularly high tool breakage rates, namely Suction Side Row 3, Suction Side Row 2, Stag Row 1, and Pressure Side Row 2. Figure 4.4 shows a hole from Pressure Side Row 2 between the roughing and finishing operations. While initially surprising, it was found that this shallow hole was intentionally programmed to reduce chipping on the overhang angle of the hole.

Figure 4.4: Diffuser hole on Pressure Side Row 2 after the roughing tool and before the finishing tool. Chipping from the current manufacturing process is highlighted.

While this approach may protect the ceramic, it forces the finishing tool to cut all the René N4, which may explain the accelerated tool wear. An analysis of the CAM toolpaths supported that the roughing tool was not being used as much as possible. Figure 4.5 is the toolpaths of both tools for a hole from Pressure Side Row 2.

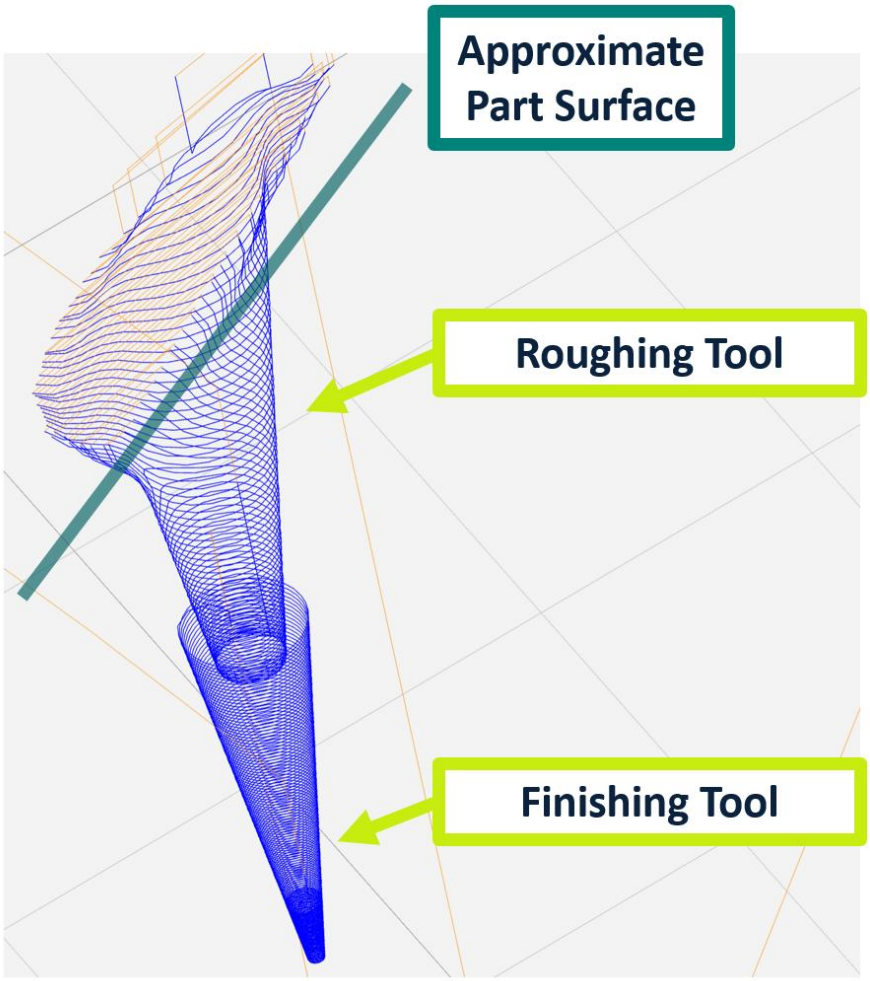

Figure 4.5: CAM toolpath of a hole on Pressure Side Row 2. A helical toolpath is shown for the roughing tool and another for the finishing tool. The tip of the tool follows the blue path.

Another factor contributing to this issue may be the variability in the ceramic coating thickness. Because the RoboDrill probes the surface of the blade to locate the part, inconsistent coating thickness can lead to an inaccurate understanding of the true geometry of the part. This may cause the finishing tool to machine through more metal than expected.

This finding suggests that further testing on CAM optimization may yield promising results. Chapter 5 will experiment on adjusting the hole-depth of the roughing tool, copying the tool wear measurement methodology developed in this chapter.

4.4 Pre-Breakage Indicators

One of the goals of this project was to determine whether any signals could be detected before catastrophic tool breakage. Although the hole-by-hole wear tracking experiment in this

chapter did not reveal any clear pre-breakage indicators, it confirmed that the tools are operating under suboptimal conditions. The limitation of only being able to measure tool length after each hole highlights the need for in-situ monitoring. The ability to recognize failures as they occur would greatly improve the ability to both improve the process and reduce process time.

To address this challenge, Luke Placzek [8] developed a framework for real-time breakage detection. His work serves as the foundation for a machine learning model that will attempt to enable predictive maintenance and intelligent process control. Although the present study does not include the completed machine learning model, the data infrastructure and signal collection has been established.

Placzek [8] integrated a hydrophone into the machine environment to record audio signatures during the cutting process. Unlike a typical microphone, the hydrophone works through contact with a surface. While this is typically water, this study used it in contact with the frame of the RoboDrill. The contact allowed it to get a high-resolution audio recording that is not possible with traditional microphones due to excess noise from the factory. Preliminary data, shown in Figure 4.6, includes the raw waveform from one hole as well as the calculated spectrogram.

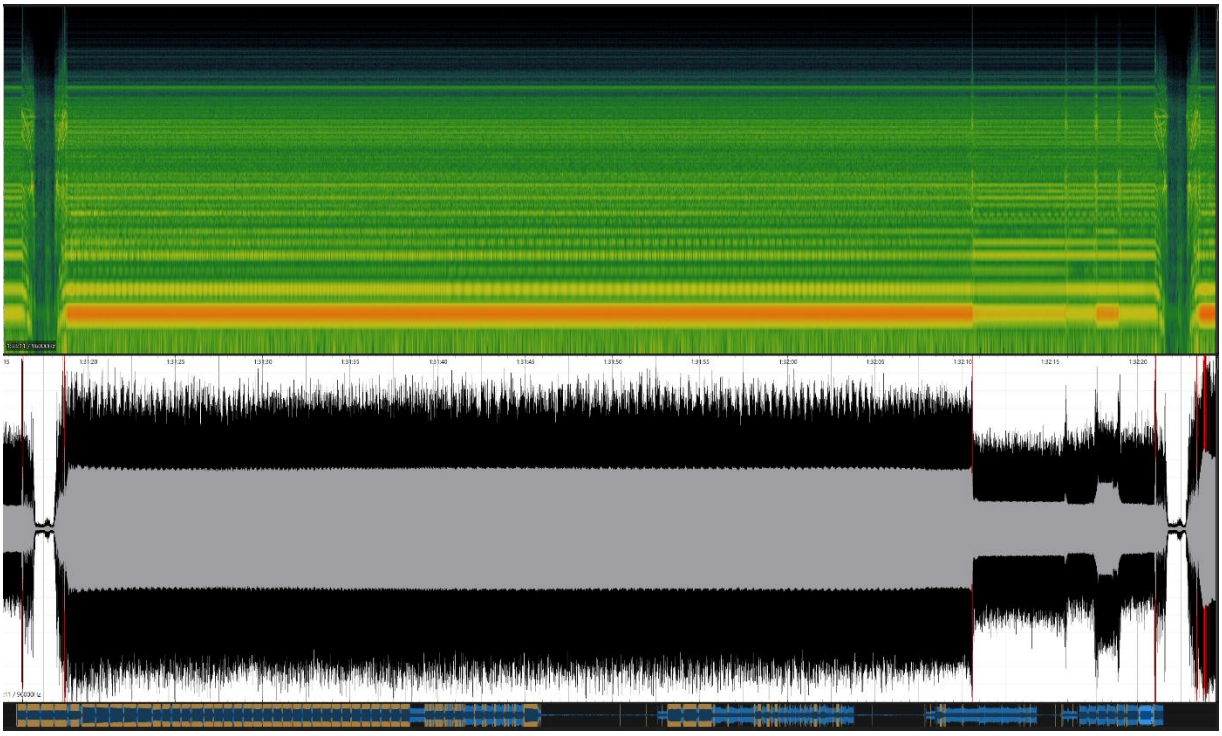

Figure 4.6: Raw waveform (bottom) and spectrogram (top) of cutting noise for one hole.

In parallel with the acoustic analysis, Placzek [8] discusses a live machine dashboard using a data platform called Vimana[1]. This dashboard is seen in Figure 4.7. This dashboard provides real-time output of machine parameters and removes the need to stop machines to extract data logs. This dashboard displays more information than is available from standard data logs. Correlating this dashboard with the acoustic data, Placzek developed a script to segment the audio data. Figure 4.8 and Figure 4.9 show audio recordings over several hours of machining, segmented using the data from Vimana. These segmented audio files will serve as training data for a supervised learning model to attempt to identify breakage conditions from sound alone.

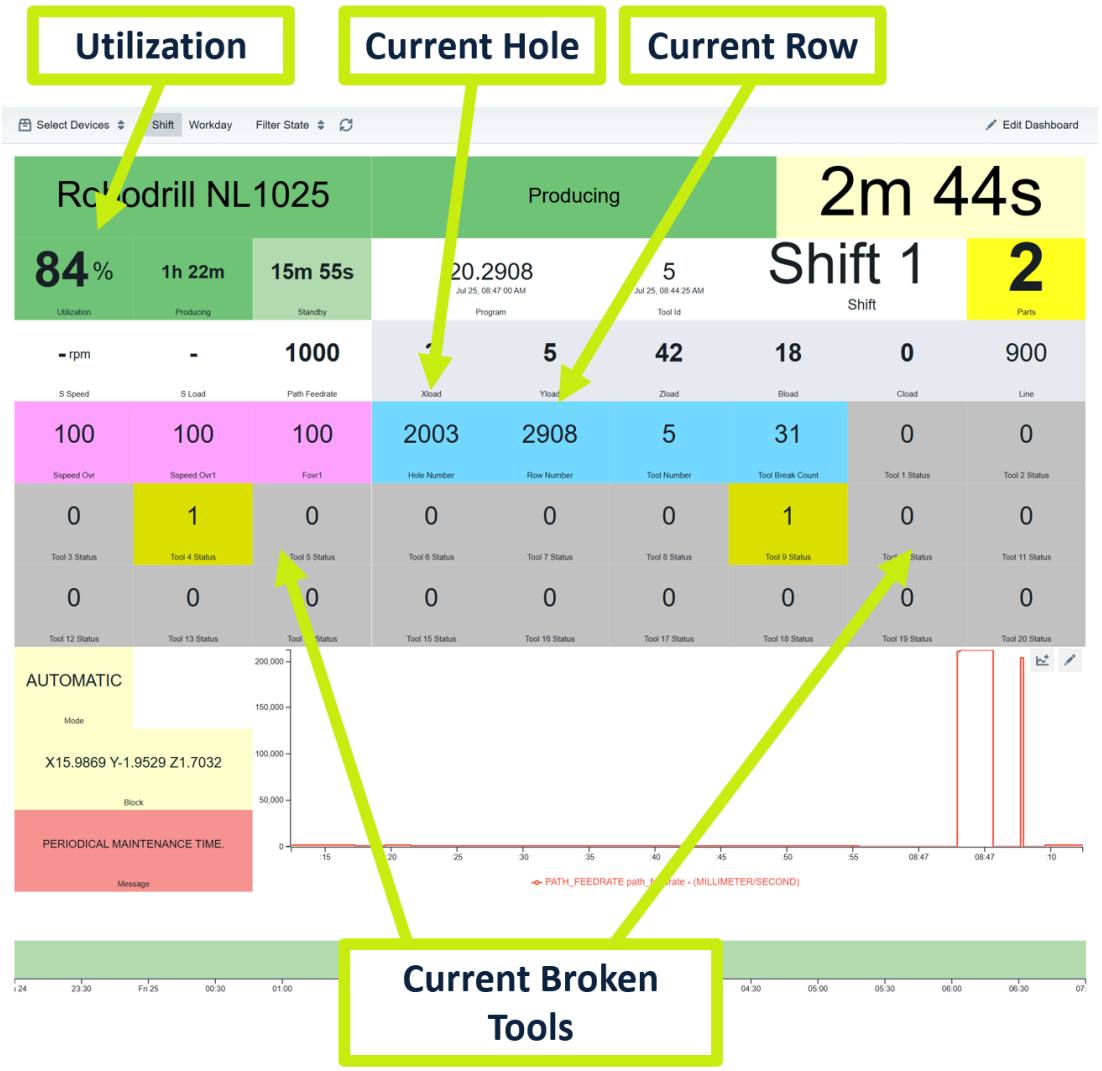

Figure 4.7: Vimana live data dashboard connected to a RoboDrill.

[1] Company information available at: https://govimana.com/

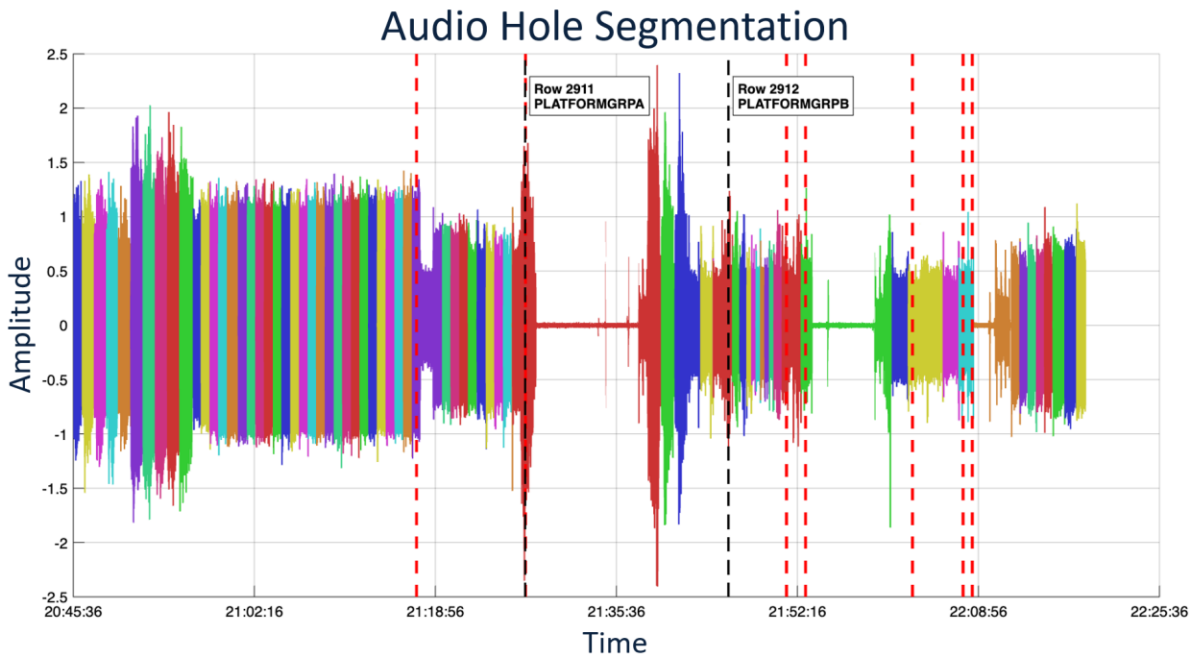

Figure 4.8: Waveform segmented into holes using Vimana data.

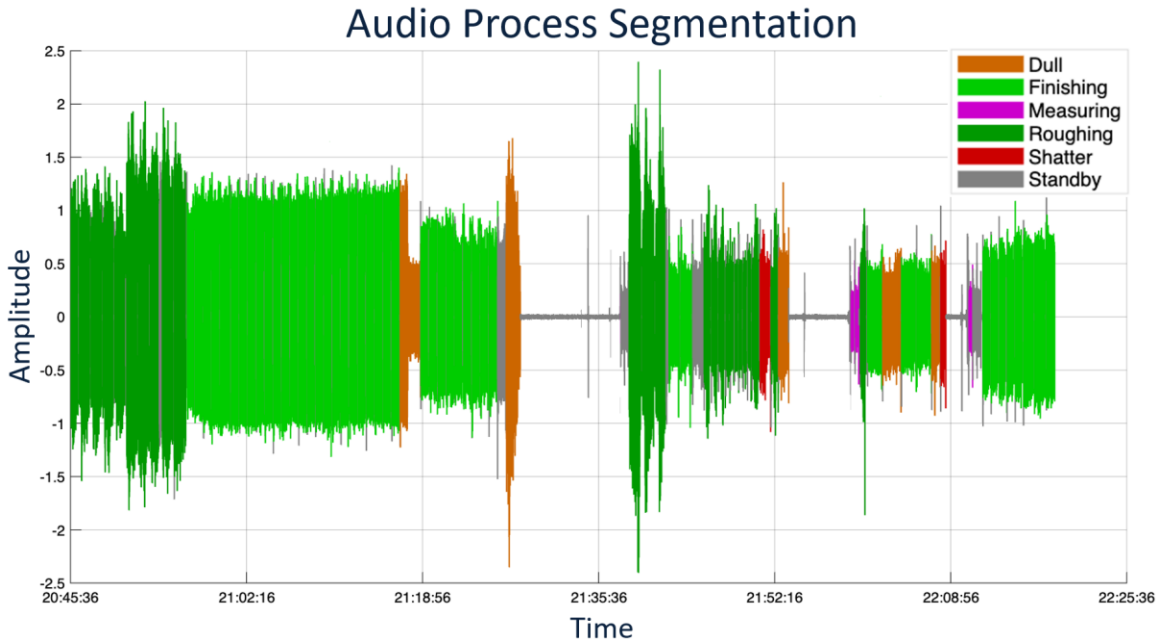

Figure 4.9: Waveform segmented into process steps using Vimana data.

Further, a live statistical process control dashboard was developed. This can be seen in Figure 4.10. This dashboard connects to the Vimana API to access both live and historical data

from the RoboDrills. This dashboard applies the Nelson Rules[2] to automatically flag when the process is behaving abnormally from a statistical perspective [28]. On this dashboard, the run chart can be filtered by machine, row, or tool type, allowing for an in-depth look at what part of the process is not functioning properly. This dashboard also implements process changes, tracked through a change log in excel. Engineers can log modifications such as code updates or tooling changes and have those changes reflected on the dashboard as a vertical line. This allows users to correlate process changes with shifts in performance, which was previously untracked.

Figure 4.10: Statistical process control dashboard for tools broken during DTC process. Each data entry is the total number of tools broken on a machined part.

Together, these tools support the documentation and classification of the tool breakage issue, allowing for tailored solutions to the problem. With continued development by GE Vernova, the acoustic data will be used to train a machine learning model. The goal is to detect failure conditions during the process which would allow for automatic intervention and rapid diagnosis. This would also help pinpoint where the tools commonly break within the hole, which is one limitation of the work done in this thesis.

[2] The Nelson Rules are used to detect when data is behaving non-randomly when compared to the mean and standard deviation of historical data.

This page was intentionally left blank

Chapter 5 Updated Toolpath Experimentation

5.1 Motivation and Context

The preceding chapter revealed that on certain problematic rows the roughing tool does not cut into the underlying René N4 at all. Instead, it only machines the ceramic coating, leaving a disproportionately high amount of material to be removed by the finishing tool. This chapter explores whether changes to cutting strategy can lead to improved tool life through an experiment where the hole made by the roughing tool is deepened. This experiment will focus on the problematic rows identified in previous chapters and the analysis will be done on holes shown to behave similar to each other as to not introduce any unnecessary nuisance variables.

5.2 Experimental Setup: Updated CAM Toolpaths

This experiment aimed to improve tool life by updating the CAM toolpaths to extend the cutting region of the roughing tool. This experiment followed the same process as the tool life wear test from Chapter 4, where tools are measured after each hole to characterize wear. The updated roughing toolpaths for this experiment were programmed to continue along the helical path until reaching a 0.010 inches final diameter. This matches the final diameter milled by this tool in other rows across the turbine blade. This modification increased the depth of each hole milled by the roughing tool by 0.070 inches, a significant adjustment which greatly reduced the volume of material removed by the finishing tool. An example of the original and updated toolpath is shown in Figure 5.1.

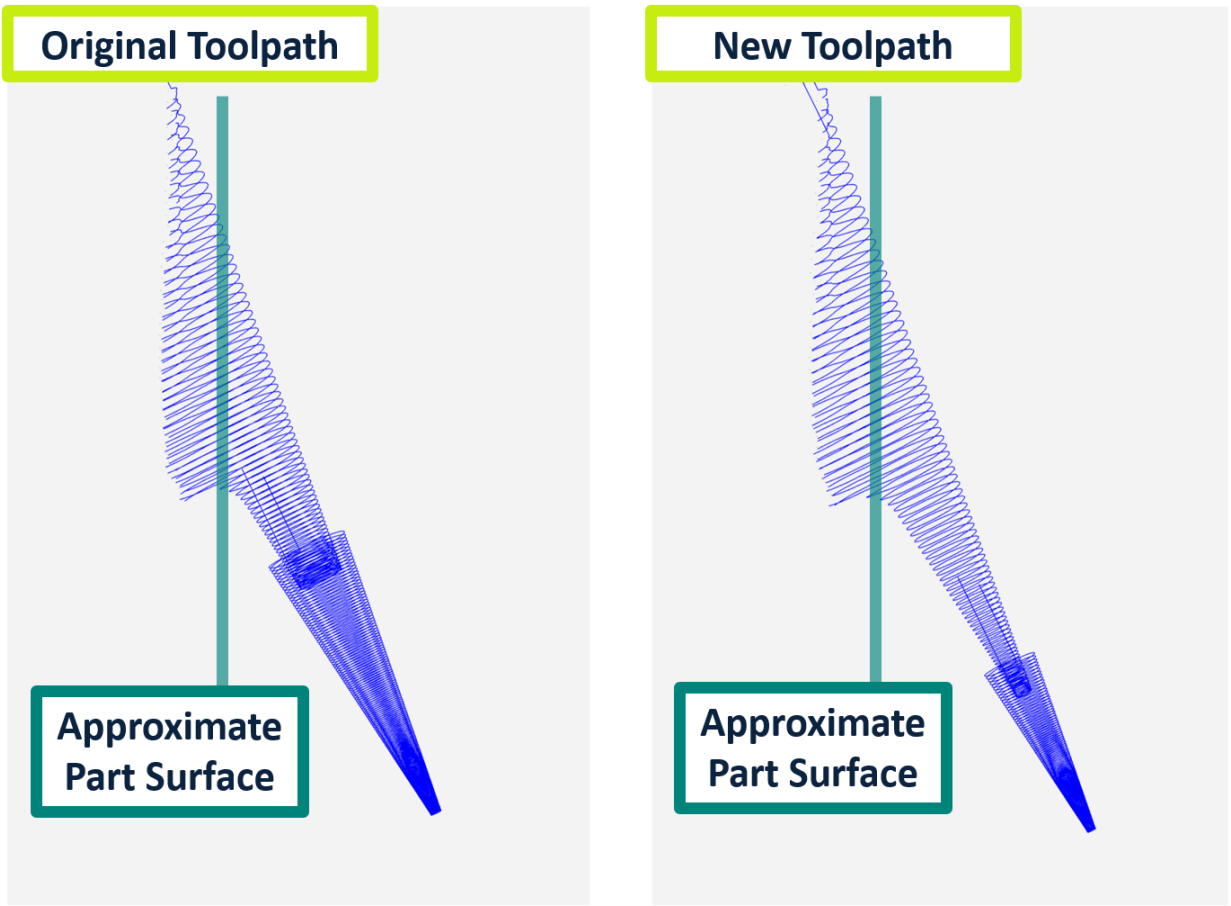

Figure 5.1: Original (left) and updated (right) CAM toolpath. This update kept the same hole geometry but extended the depth of the hole that was milled by the roughing tool.

Because the manufacturing process is frozen, this test could not be conducted on production parts. Instead, a scrapped turbine blade was repurposed for this experiment. The scrap part already had all the holes machined into it, and therefore the updated toolpaths also had to be moved to a different place on the blade. For each row, the holes were offset to be cut between existing rows. This offset is seen in Figure 5.2.

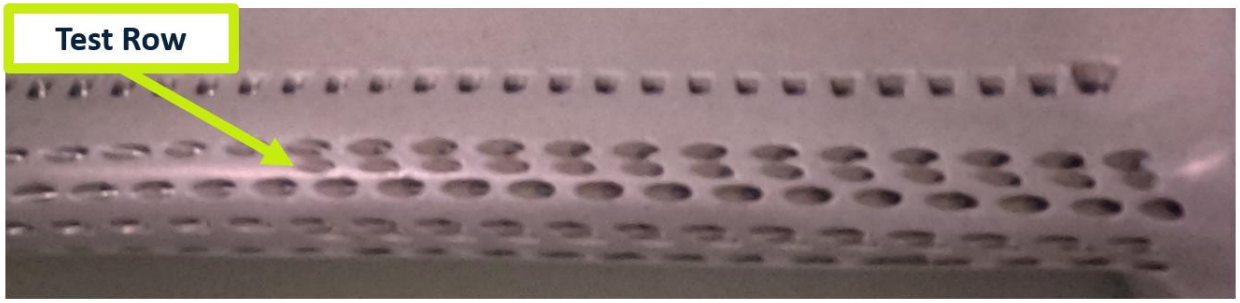

Figure 5.2: Hole offset for experiment on scrap part.

This experiment focused on holes 11 through 23 across Suction Side Row 3, Suction Side Row 2, and Pressure Side Row 2. These rows were selected based on the work done in prior chapters. It is assumed that offsetting the holes does not significantly change the tool performance. Additionally, this test was run on a newly installed machine that has not yet entered production. This introduces the assumption that the machine's performance is representative of the other machines. To implement the results from this test into production, further testing will need to be done to ensure that the results are consistent across machines.

5.3 Wear Progression Results

In this experiment, the depth of the hole machined by the roughing tool was extended, as shown in Figure 5.1. However, the wear of the roughing tool was not measured after each hole. This was decided because the roughing tool was not predicted to break many times and repeatedly measuring it would significantly increase experimental time. Additionally, since this experiment was performed on scrap blades and required offset holes, the roughing toolpath overlapped with pre-existing holes on the blade. An image of the overlap is shown in Figure 5.3. This was not intended, but a result of the RoboDrill failing to accurately locate the part because the RoboDrill probe occasionally contacted the blade where a hole had already been milled, which offset the expected surface location of the part. This overlap means that the wear of the roughing tool from this experiment does not perfectly represent how the tool would wear if this were done on a production part. However, the selected holes were machined on two scrap blades, and only one hole caused a roughing tool to break. This breakage rate is consistent with historical data.

Figure 5.3: Experimental hole overlapping with existing hole.

Despite the holes overlapping, the roughing tool cut into both the ceramic and metal, with the bottom of the hole never overlapping with existing holes. This ensured that the finishing tool followed its entire programmed path without having that portion of the hole affected by existing holes on the blade.

The life of the finishing tools notably improved in this test when compared to historical data. Chapter 3 indicated that medium length finishing tools had a life of three holes on average before catastrophic failure. During this experiment, the shortest observed tool life was seven holes, while every other tool lasted between 10 and 14 holes. Figure 5.4 and Figure 5.5 show the wear progression curves for each finishing tool used in the experiment, with each figure showing results from a scrapped turbine blade. While the general wear trends follow expectations, there are a few instances where the plots show a tool wearing on a hole and then appearing longer in the following measurement. This is physically impossible and most likely due to coolant interfering with the laser measurement. Despite this, the overall results clearly show an increase in tool life.

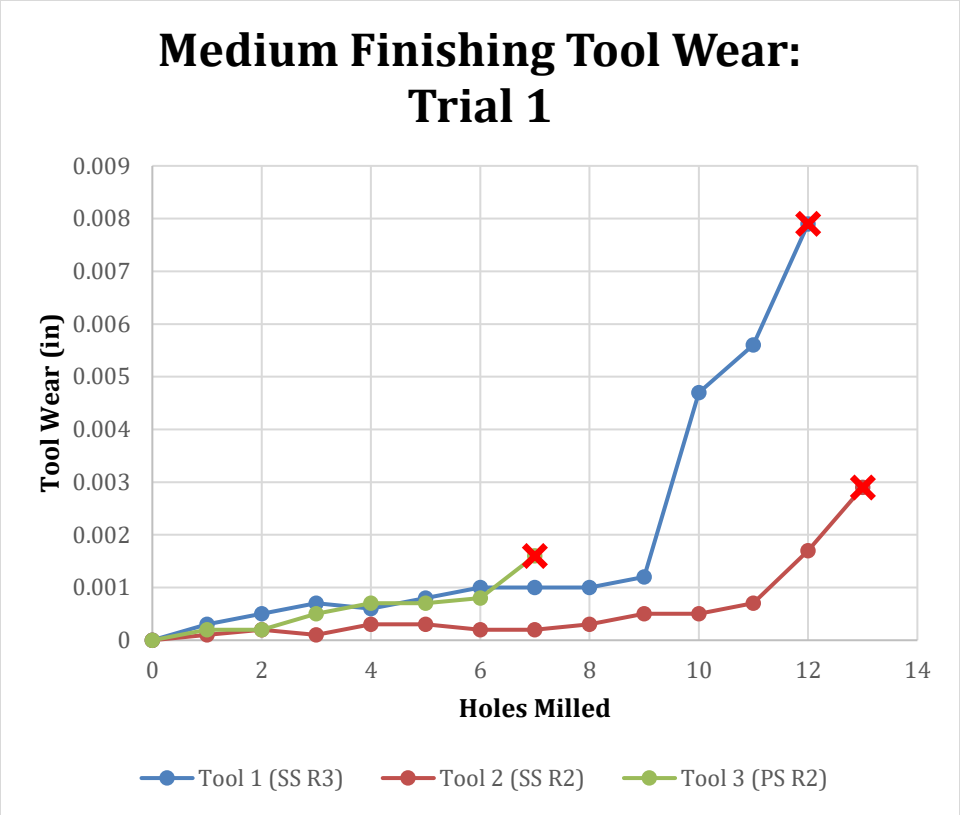

Figure 5.4: Medium length finishing tool wear plotted across holes on a scrap blade. This tool wear is significantly improved due to the updated CAM. The "X" denotes the last successful hole machined before the tool wore by 0.008 inches.

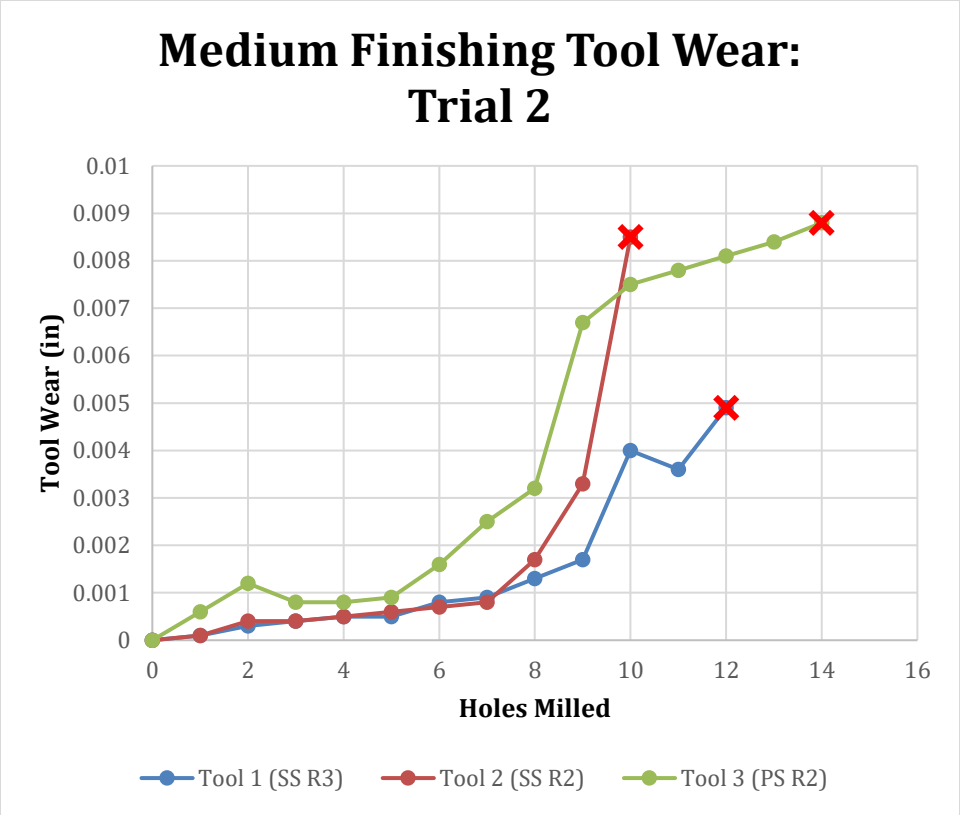

Figure 5.5: Medium length finishing tool wear plotted across holes on a second scrap blade. This tool wear is significantly improved due to the updated CAM. The "X" denotes the last successful hole machined before the tool wore by 0.008 inches.

It should also be noted that a few tools appeared to wear more than 0.008 inches, which is the threshold set on the RoboDrill to detect a breakage. In this experiment the RoboDrill checked if each tool was broken before it was manually programmed to measure a tool. If the tool was not flagged as broken, it was measured and the experiment was continued. Once again, coolant likely added inaccuracy to the laser. Regardless, if the machine did not flag the tool as broken it would have continued to be used in production, and therefore the number of holes milled until flagged as broken is the most meaningful indicator of tool life improvement.

Chapter 6 Conclusion and Future Work

6.1 Findings and Recommendations for Manufacturing

This thesis identified and addressed key factors driving premature tool breakage in the small-diameter machining of nickel-based superalloys. The study began by systematically documenting tool breakage modes through a photographic analysis. This was supplemented with an analysis of production data, plotting trends across holes and rows, revealing mistakes in the current CAM programming of certain holes. The overall analysis also revealed that several finishing tools were breaking disproportionately more than the other tool types. Additionally, these breakages were not uniform across the blade. Suction Side Row 3, Suction Side Row 2, Stag Row 1, and Pressure Side Row 2 were shown to be the most problematic rows. A statistical analysis showed that Suction Side Row 3, Suction Side Row 2, and Pressure Side Row 2 behaved similarly enough in terms of tool breakage frequency to be treated as a group in experimentation. This discovery allowed for targeted process improvement without the need to experiment across many blades to have enough data.

Tool wear progression testing provided additional insight into why the identified problematic rows performed so poorly. It was discovered that on the problematic rows, the roughing tool was not fully cutting through the ceramic coating, leaving the underlying René N4 untouched. The volume of material removed by the finishing tool was larger on these rows than others resulting in accelerated wear per hole. To address this, an updated CAM strategy was developed which extended the depth of the hole machined by the roughing tool, arriving at a final diameter comparable to other rows. Although this test was performed on a new machine and scrapped turbine blades, it clearly improved tool life. Prior to this change, the four problematic rows averaged four medium length finishing tools broken per row. The results from this test estimate that the improved CAM will only break one medium length finishing tool per row. Extrapolating this improvement to the upper half of each row would similarly reduce breakage, allowing the short length finishing tool to be replaced only once per row instead of twice.

Across production, this solution equated to approximately 16 fewer tool replacements per part. The two CAM mistakes fixed in Chapter 3 results in an additional two tools saved. With tools costing roughly $19 each and 20 machines running continuously and producing parts every 24 hours, the projected savings are approximately $2.5 million per year. This estimate does not account for additional profit potential from the reduction in cycle time. The implementation risk is minimal because there is no added process complexity or tooling requirements. By simultaneously deploying the proactive monitoring tools developed by Placzek [8], GE Vernova can ensure that these improvements are sustained, measurable, and adaptable to future changes in the process.

6.2 Future Work

One unresolved finding from this study was the unusually low tool breakage frequency of machine NL1025. While subsequent data obtained at the end of the study indicated that its performance has become more in line with other machines, the root cause of the initial performance remains unknown. Further targeted investigation into this anomaly may uncover additional best practices or maintenance actions that could be applied to all machines.

While the results of the updated CAM strategy are highly encouraging, several steps remain before the change can be fully validated for production deployment. First, the updated toolpaths should be run on new parts instead of scrap parts to confirm that the observed benefits in tool life translate to production. This will also ensure that the modified roughing strategy produces holes that remain within all the dimensional and quality specification limits. Before implementation into production, a formal verification process will need to be performed on a part machined with the updated process.

During the trials of the experimental CAM toolpaths, minor chipping of the ceramic was observed in some holes. This was most likely caused by the overlap of experimental holes and existing holes, resulting in exceedingly thin ceramic regions, but nevertheless it is worth confirming that such chipping does not occur under standard production conditions. The most pressing future work to be done by GE Vernova is confirming the updated CAM benefits and applying it to the production line.

Appendix A: Tool Images and Measurements

Table A.1: Breakage photos and characterization of 30 random roughing tools.

Photo	Index	Length (in)	Breakage Type	Notes
	NEW TOOL			
	1	1.4975	Dull	
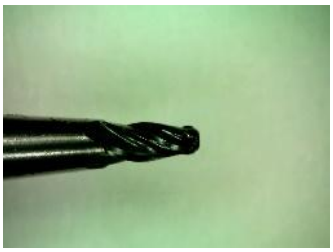	2	1.492	Dull	Flat tip
	3	1.431	Melt	
	4	1.494	Dull	

	5	1.432	Shatter	
	6	1.5015	Dull	Still pointed but missing indents
	7	1.4735	Melt	
	8	1.474	Melt	
	9	1.5035	Looks New	

	10	1.469	Shatter	
	11	1.414	Shatter	
	12	1.4995	Dull	Maybe looks new
	13	1.5035	Looks New	
	14	1.4885	Melt	Bad photo

	15	1.382	Shatter	
	16	1.3855	Shatter	
	17	1.476	Melt	
	18	1.488	Dull	Looks flat - Bad photo
	19	1.498	Dull	Bad photo

	20	1.501	Looks New	Maybe dull
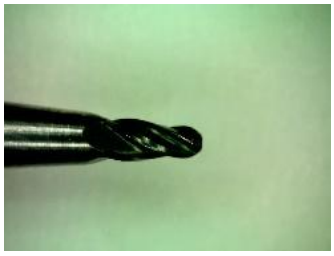	21	1.4925	Dull	
	22	1.4905	Dull	Looks flat
	23	1.46	Melt	
	24	1.495	Dull	

	25	1.478	Melt	
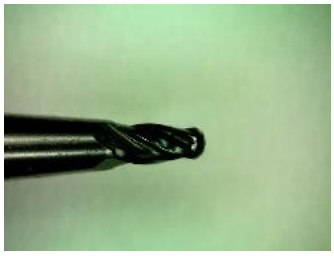	26	1.4865	Melt	
	27	1.442	Shatter	Odd bump on end of bit
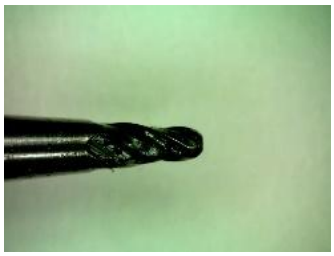	28	1.4995	Dull	
	29	1.4995	Dull	

	30	1.502	Dull	Close to new

Table A.2: Breakage photos and characterization of 30 random finishing tools.

Photo	Index	Length (in)	Breakage Type	Notes
	NEW TOOL			
	1	1.343	Shatter	
	2	1.374	Shatter	
	3	1.331	Shatter	No photo
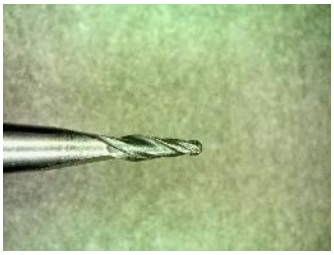	4	1.487	Dull	

	5	1.43	Shatter	Chip in the side of the flute
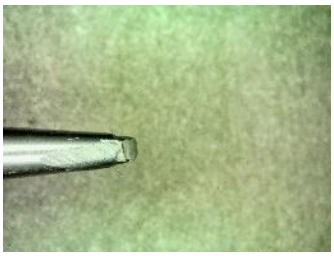	6	1.4065	Shatter	
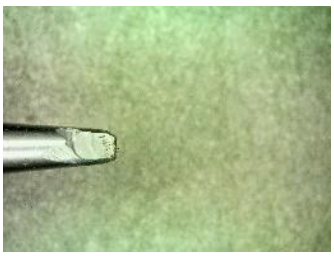	7	1.383	Shatter	
	8	1.4185	Shatter	Chip in the side of the flute
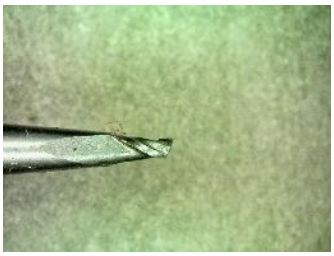	9	1.449	Shatter	

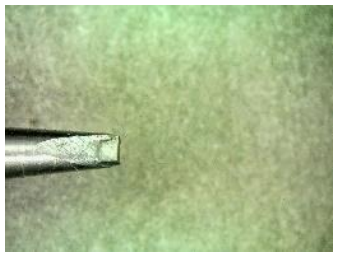	10	1.38	Shatter
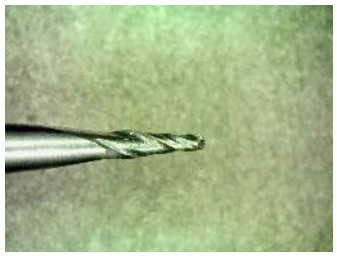	11	1.4925	Dull
	12	1.48	Dull
	13	1.5065	Looks new
	14	1.403	Shatter

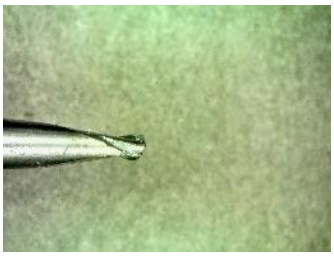	15	1.4235	Shatter
	16	1.3875	Shatter
	17	1.487	Shatter
	18	1.3985	Shatter
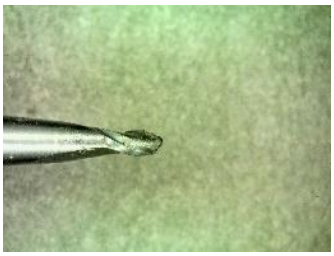	19	1.44	Shatter

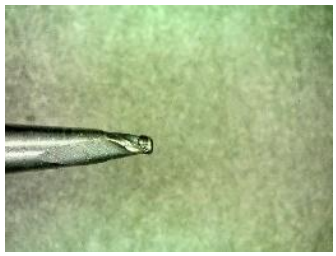	20	1.435	Shatter	Shatter then melt
	21	1.382	Shatter	
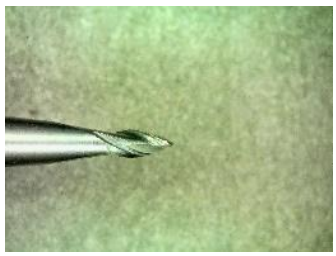	22	1.4505	Shatter	
	23	1.408	Shatter	Interesting crack propagation up shaft
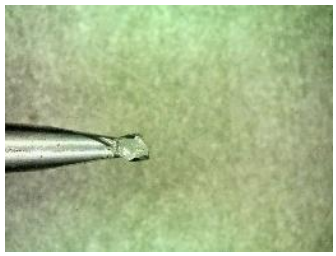	24	1.42	Shatter	

	25	1.479	Dull	
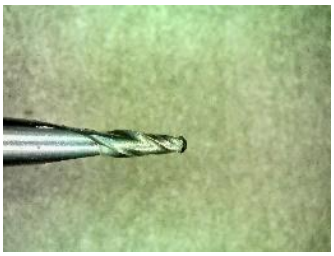	26	1.476	Melt	
	27	1.4205	Shatter	
	28	1.379	Shatter	
	29	1.501	Dull	Maybe new

	30 1.503 Looks new

Appendix B: RoboDrill Dashboard Plots

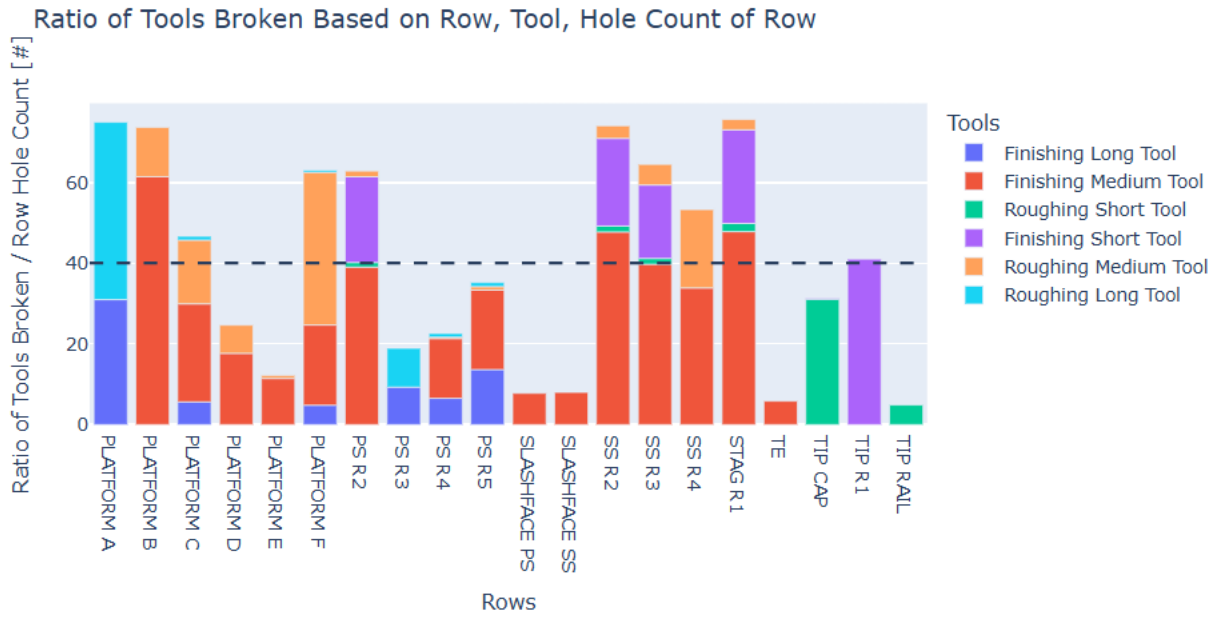

Figure B.1: Bar chart of total tool breakage by row, segmented by tool type and normalized by hole count per row.

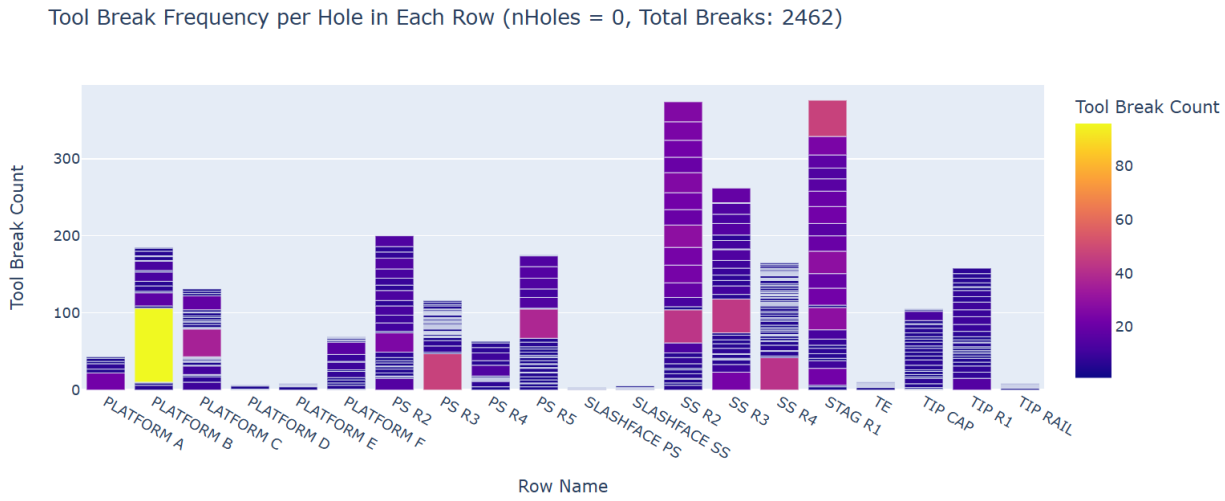

Figure B.2: Bar chart of tools broken by row with an operational life of one hole, segmented by hole.

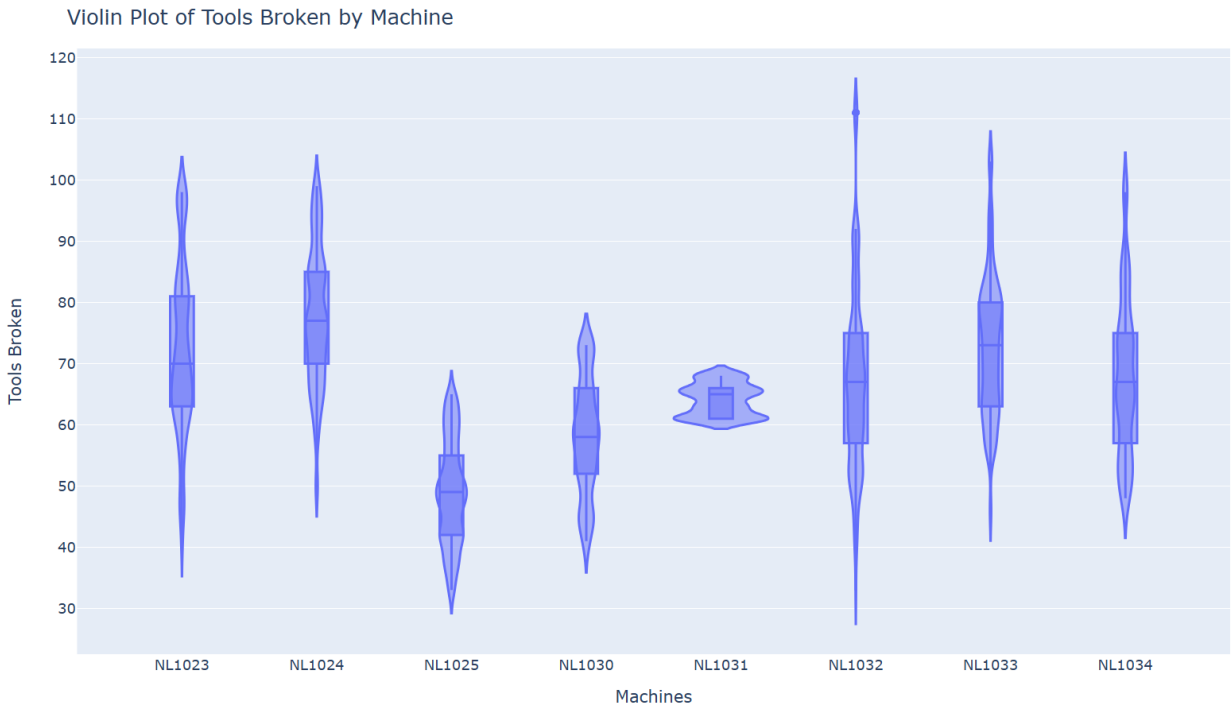

Figure B.3: Violin plot of average number of tools broken per part by each machine.

Appendix C: Statistical Tables

Table C.1: One-way ANOVA table comparing average tool breakage between machines.

DESCRIPTION						Alpha	0.05	
Group	*Count*	*Sum*	*Mean*	*Variance*	*SS*	*Std Err*	*Lower*	*Upper*
NL 1023	10	584	58.4	110	992	3.27	51.8	65.0
NL 1024	10	726	72.6	113	1020	3.27	66.0	79.2
NL 1025	10	419	41.9	45.7	411	3.27	35.3	48.5
NL 1032	10	528	52.8	126	1130	3.27	46.2	59.4
NL 1033	10	663	66.3	125	1130	3.27	59.7	72.9
NL 1034	10	676	67.6	120	1080	3.27	61.0	74.2

ANOVA

Sources	*SS*	*df*	*MS*	*F*	*P value*	*Eta-sq*	*RMSSE*	*Omega Sq*
Between Groups	6380	5	1280	12.0	8.2E-08	0.525	1.09	0.477
Within Groups	5760	54	107					
Total	12100	59	206					

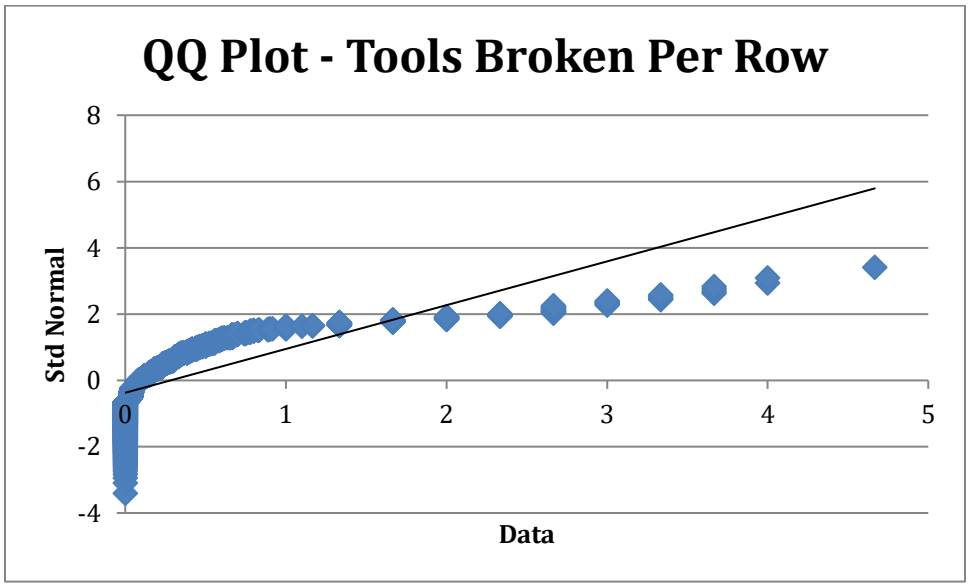

Figure C.1: Q-Q plot of tools broken per part normalized by hole count per row.

Table C.2: Group characterization calculations for DUNN test on machine NL1023.

DUNN's TEST			alpha	0.05	0.000263
group	*R-sum*	*size*	*R-mean*	*z-crit*	
TIP RAIL	596	10	59.6		
SS R3	1621	10	162.1		
SS R2	1503.5	10	150.35		
STAG R1	1755	10	175.5		
PS R2	1452.5	10	145.25		
TIP R1	1035	10	103.5		
SS R4	1188.5	10	118.85		
PS R3	1027	10	102.7		
PS R4	808	10	80.8		
PLAT A	727	10	72.7		
PLAT B	1486	10	148.6		
PLAT C	1234	10	123.4		
PLAT D	727	10	72.7		
PLAT E	433	10	43.3		
PLAT F	1292.5	10	129.25		
SLASH					
SS	401	10	40.1		
SLASH					
PS	571	10	57.1		
PS R5	1013	10	101.3		
TE	367	10	36.7		
TIP CAP	862	10	86.2		
		200		1.96	

Table C.3: Significant row pairs from DUNN test on machine NL1023.

D TEST						
group 1	*group 2*	*R-mean*	*std err*	*z-stat*	*R-crit*	*p-value*
TIP RAIL	SS R3	103	25.6	4.00	50.2	6.27E-05
TIP RAIL	STAG R1	116	25.6	4.53	50.2	6.02E-06
SS R3	PLAT E	119	25.6	4.64	50.2	3.50E-06
SS R3	SLASH SS	122	25.6	4.76	50.2	1.90E-06
SS R3	SLASH PS	105	25.6	4.10	50.2	4.13E-05
SS R3	TE	125	25.6	4.90	50.2	9.75E-07
SS R2	PLAT E	107	25.6	4.18	50.2	2.91E-05
SS R2	SLASH SS	110	25.6	4.31	50.2	1.67E-05
SS R2	TE	114	25.6	4.44	50.2	9.09E-06
STAG R1	PS R4	94.7	25.6	3.70	50.2	0.000217
STAG R1	PLAT A	103	25.6	4.01	50.2	5.96E-05
STAG R1	PLAT D	103	25.6	4.01	50.2	5.96E-05
STAG R1	PLAT E	132	25.6	5.16	50.2	2.44E-07
STAG R1	SLASH SS	135	25.6	5.29	50.2	1.24E-07
STAG R1	SLASH PS	118	25.6	4.62	50.2	3.78E-06
STAG R1	TE	139	25.6	5.42	50.2	5.96E-08
PS R2	PLAT E	102	25.6	3.98	50.2	6.86E-05
PS R2	SLASH SS	105	25.6	4.11	50.2	4.03E-05
PS R2	TE	109	25.6	4.24	50.2	2.25E-05
PLAT B	PLAT E	105	25.6	4.111	50.2	3.93E-05
PLAT B	SLASH SS	109	25.6	4.24	50.2	2.27E-05
PLAT B	TE	112	25.6	4.37	50.2	1.25E-05

This page was intentionally left blank

Appendix D: Tool Wear Raw Data

Table D.1: Tool life wear test lengths and images for medium length finishing tool machining suction side row 4.

Hole	Starting Length (in)	Length after Hole (in)	Delta Length (in)	End Mill Photo	Hole Photo
			NEW TOOOL		
1	7.5785	7.5781	0.0004	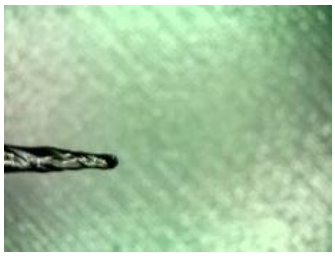	
2	7.5785	7.5778	0.0007	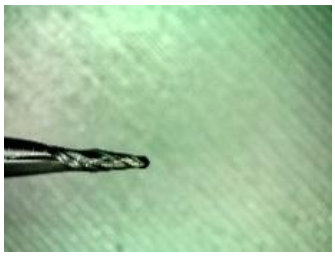	
3	7.5785	7.5779	0.0006	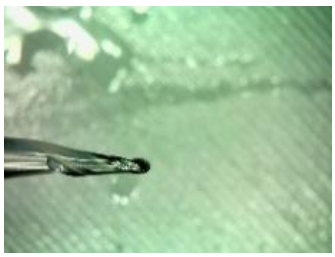	

4	7.5785	7.5777	0.0008	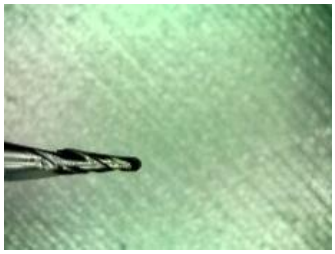	
5	7.5785	7.5776	0.0009	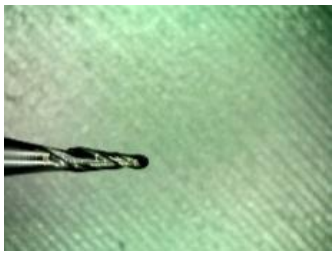	
6	7.5785	7.5776	0.0009	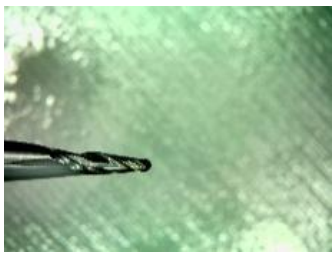	
7	7.5785	7.5776	0.0009	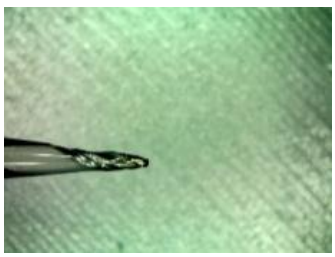	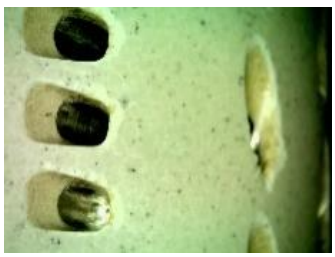
8	7.5785	7.5775	0.001		
9	7.5785	7.5773	0.0012	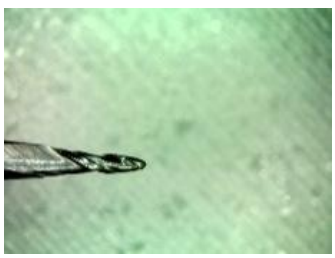	

10	7.5785	7.5772	0.0013	[No photo]	[No photo]

Table D.2: Tool life wear test lengths and images for medium length roughing tool machining suction side row 4.

Hole	Starting Length (in)	Length after Hole (in)	Delta Length (in)	End Mill Photo	Hole Photo
			NEW TOOL		
1	7.4677	7.4651	0.0026	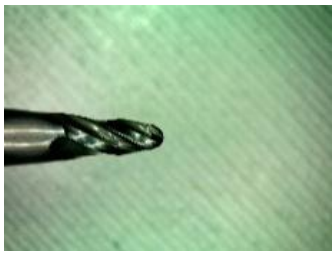	
2	7.4677	7.4651	0.0026		
3	7.4677	7.4651	0.0026		
4	7.4677	7.465	0.0027	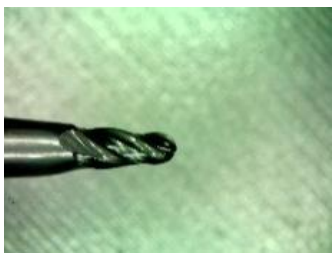	

5	7.4677	7.4649	0.0028	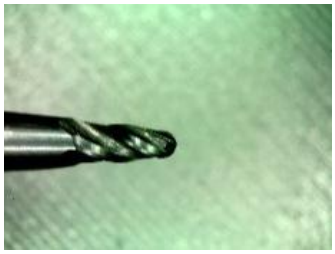	
6	7.4677	7.4648	0.0029	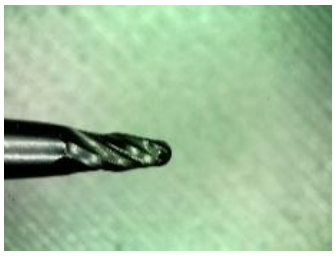	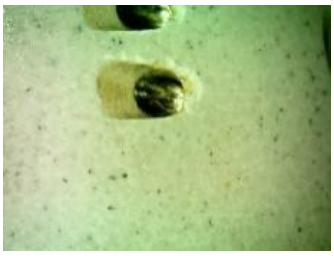
7	7.4677	7.4647	0.003	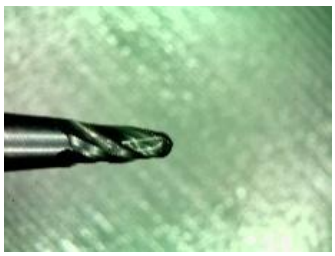	
8	7.4677	7.4647	0.003	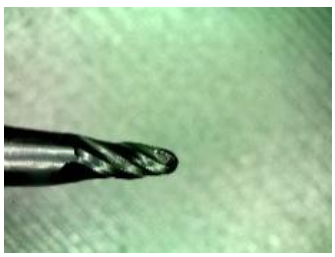	
9	7.4677	7.4646	0.0031		
10	7.4677	7.4644	0.0033	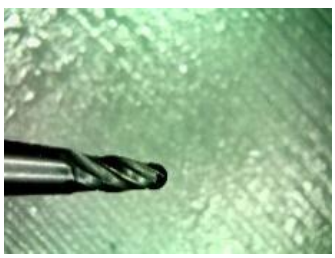	

11	7.4677	7.4644	0.0033	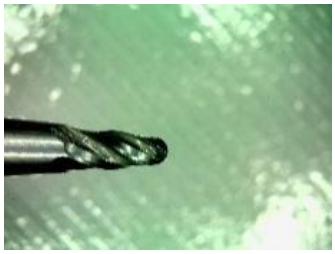	
12	7.4677	7.464	0.0037	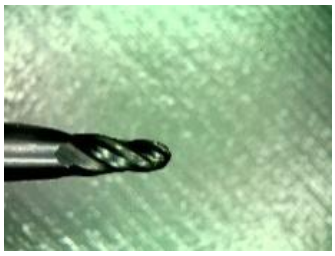	
13	7.4677	7.4637	0.004	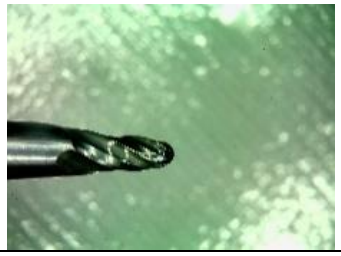	

Table D.3: Tool life wear test lengths and images for medium length finishing tool machining stag row 1.

Hole	Starting Length (in)	Length after Hole (in)	Delta Length (in)	End Mill Photo	Note
			NEW TOOL		
1	7.5111	7.5088	0.0023	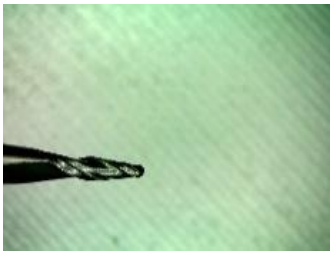	
2	7.5111	7.5079	0.0032	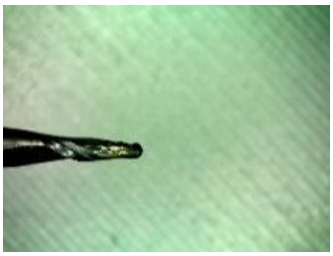	
3	7.5111	7.4999	0.0112	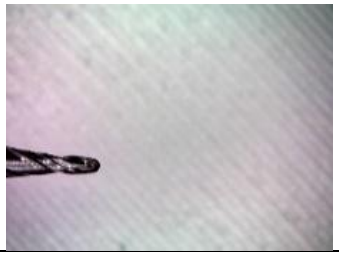	Failure: dull

4	7.5048	7.5023	0.0025	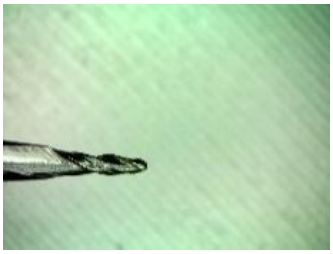	
5	7.5048	7.4943	0.0105		Failure: shatter
6	7.5716	7.5692	0.0024		
7	7.5716	7.5682	0.0034	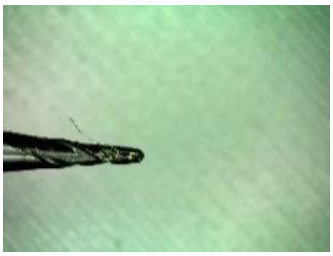	
8	7.5716	7.5602	0.0114	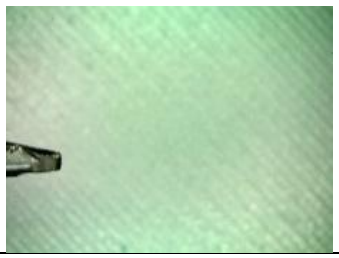	Failure: shatter

9	7.5987	7.596	0.0027		
10	7.5987	7.5954	0.0033	[No photo]	
11	7.5987	7.5947	0.004	[No photo]	
12	7.5987	7.5867	0.012	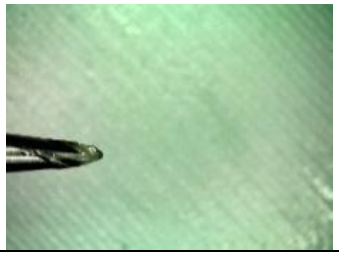	Failure: shatter

This page was intentionally left blank

References

[1] M. Quesnel, “GE’s HA Gas Turbine Delivers Second World Record for Efficiency | GE News.” Accessed: Jun. 21, 2025. [Online]. Available: https://www.ge.com/news/press-releases/ges-ha-gas-turbine-delivers-second-world-record-efficiency

[2] S. M. Meier and D. K. Gupta, “The Evolution of Thermal Barrier Coatings in Gas Turbine Engine Applications,” *J. Eng. Gas Turbines Power*, vol. 116, no. 1, pp. 250–257, Jan. 1994, doi: 10.1115/1.2906801.

[3] A. Giorgetti, C. Monti, L. Tognarelli, and F. Mastromatteo, “Microstructural evolution of René N4 during high temperature creep and aging,” *Results Phys.*, vol. 7, pp. 1608–1615, Jan. 2017, doi: 10.1016/j.rinp.2017.04.027.

[4] E. O. Ezugwu, Z. M. Wang, and A. R. Machado, “The machinability of nickel-based alloys: a review,” *J. Mater. Process. Technol.*, vol. 86, no. 1, pp. 1–16, Feb. 1999, doi: 10.1016/S0924-0136(98)00314-8.

[5] H. Zhang, Y. Gong, C. Liang, Y. Sun, and J. Zhao, “Study on milling material removal mechanism and surface integrity of nickel-based single crystal superalloy DD5,” *Int. J. Adv. Manuf. Technol.*, vol. 125, no. 5–6, pp. 2323–2338, 2023, doi: 10.1007/s00170-022-10448-0.

[6] B. Denkena *et al.*, “Influence of tool material properties on the wear behavior of cemented carbide tools with rounded cutting edges,” *Wear*, vol. 456–457, p. 203395, Sep. 2020, doi: 10.1016/j.wear.2020.203395.

[7] N. Chen *et al.*, “Advances in micro milling: From tool fabrication to process outcomes,” *Int. J. Mach. Tools Manuf.*, vol. 160, p. 103670, Jan. 2021, doi: 10.1016/j.ijmachtools.2020.103670.

[8] L. Placzek, “Enabling deep learning for acoustic condition monitoring in machining superalloy turbine blades,” MEng Thesis, Massachusetts Institute of Technology.

[9] D. Huo, *Micro-Cutting: Fundamentals and Applications*. John Wiley & Sons, 2013.

[10] M. P. Vogler, R. E. DeVor, and S. G. Kapoor, “On the Modeling and Analysis of Machining Performance in Micro-Endmilling, Part I: Surface Generation,” *J. Manuf. Sci. Eng.*, vol. 126, no. 4, pp. 685–694, Nov. 2004, doi: 10.1115/1.1813470.

[11] Y.-Y. Ren, B.-G. Jia, M. Wan, and H. Tian, “Stability of Micro-Milling Tool Considering Tool Breakage,” *J. Manuf. Mater. Process.*, vol. 8, no. 3, Art. no. 3, Jun. 2024, doi: 10.3390/jmmp8030122.

[12] J. Chae, S. S. Park, and T. Freiheit, “Investigation of micro-cutting operations,” *Int. J. Mach. Tools Manuf.*, vol. 46, no. 3, pp. 313–332, Mar. 2006, doi: 10.1016/j.ijmachtools.2005.05.015.

[13] K. Zeng, X. Wu, F. Jiang, J. Shen, L. Zhu, and L. Li, “A comprehensive review on the cutting and abrasive machining of cemented carbide materials,” *J. Manuf. Process.*, vol. 108, pp. 335–358, Dec. 2023, doi: 10.1016/j.jmapro.2023.10.042.

[14] P. Piljek, Z. Keran, and M. Math, “Micromachining,” *Interdiscip. Descr. Complex Syst.*, vol. 12, no. 1, pp. 1–27, 2014, doi: 10.7906/indecs.12.1.1.

[15] B. Z. Balázs, N. Geier, M. Takács, and J. P. Davim, “A review on micro-milling: recent advances and future trends,” *Int. J. Adv. Manuf. Technol.*, vol. 112, no. 3, pp. 655–684, Jan. 2021, doi: 10.1007/s00170-020-06445-w.

[16] T. M. Moges, K. A. Desai, and P. V. M. Rao, “Improved Process Geometry Model with Cutter Runout and Elastic Recovery in Micro-end Milling,” *Procedia Manuf.*, vol. 5, pp. 478–494, Jan. 2016, doi: 10.1016/j.promfg.2016.08.040.
[17] L. Soriano Gonzalez, F. Medina Aguirre, S. L. Soo, R. Hood, and D. Novovic, “Influence of Size Effect in Milling of a Single-Crystal Nickel-Based Superalloy,” *Micromachines*, vol. 14, no. 2, Art. no. 2, Feb. 2023, doi: 10.3390/mi14020313.
[18] Q. Gao, Y. Gong, Y. Zhou, and X. Wen, “Experimental study of micro-milling mechanism and surface quality of a nickel-based single crystal superalloy,” *J. Mech. Sci. Technol.*, vol. 31, no. 1, pp. 171–180, 2017, doi: 10.1007/s12206-016-1218-y.
[19] J. Qiu, T. Yang, Z. Zhang, Q. Li, Z. Yan, and L. Wang, “On the Anisotropic Milling Machinability of DD407 Single Crystal Nickel-Based Superalloy,” *Materials*, vol. 15, no. 8, pp. 2723-, 2022, doi: 10.3390/ma15082723.
[20] M. Arif, M. Rahman, and W. Y. San, “Analytical model to determine the critical conditions for the modes of material removal in the milling process of brittle material,” *J. Mater. Process. Technol.*, vol. 212, no. 9, pp. 1925–1933, Sep. 2012, doi: 10.1016/j.jmatprotec.2012.04.014.
[21] L. Móricz, Z. J. Viharos, A. Németh, and A. Szépligeti, “Indirect measurement and diagnostics of the tool wear for ceramics micro-milling optimisation,” *J. Phys. Conf. Ser.*, vol. 1065, no. 10, pp. 102003-, 2018, doi: 10.1088/1742-6596/1065/10/102003.
[22] X. Lu, H. Zhang, Z. Jia, Y. Feng, and S. Y. Liang, “A New Method for the Prediction of Micro-Milling Tool Breakage,” in *Volume 1: Processes*, Los Angeles, California, USA: American Society of Mechanical Engineers, Jun. 2017, p. V001T02A037. doi: 10.1115/MSEC2017-2999.
[23] W. Acchar, U. U. Gomes, W. A. Kaysser, and J. Goring, “Strength Degradation of a Tungsten Carbide-Cobalt Composite at Elevated Temperatures,” *Mater. Charact.*, vol. 43, no. 1, pp. 27–32, Jul. 1999, doi: 10.1016/S1044-5803(98)00056-4.
[24] J. A. Ghani, C. H. Che Haron, S. H. Hamdan, A. Y. Md Said, and S. H. Tomadi, “Failure mode analysis of carbide cutting tools used for machining titanium alloy,” *Ceram. Int.*, vol. 39, no. 4, pp. 4449–4456, May 2013, doi: 10.1016/j.ceramint.2012.11.038.
[25] “Tool Wear - an overview | ScienceDirect Topics.” Accessed: Jul. 17, 2025. [Online]. Available: https://www-sciencedirect-com.libproxy.mit.edu/topics/mathematics/tool-wear
[26] S. Saha, S. Deb, and P. P. Bandyopadhyay, “Progressive wear based tool failure analysis during dry and MQL assisted sustainable micro-milling,” *Int. J. Mech. Sci.*, vol. 212, p. 106844, Oct. 2021, doi: 10.1016/j.ijmecsci.2021.106844.
[27] X. Zhang, M. Li, S. L. Soo, and X. Yang, “Failure characteristics and wear evolution of coated carbide tools with different geometric structures in turning GH4169 nickel-based superalloys,” *Wear*, vol. 564–565, p. 205720, Mar. 2025, doi: 10.1016/j.wear.2024.205720.
[28] L. S. Nelson, “The Shewhart Control Chart—Tests for Special Causes,” *J. Qual. Technol.*, vol. 16, no. 4, pp. 237–239, Oct. 1984, doi: 10.1080/00224065.1984.11978921.